THE ASTROPHYSICAL JOURNAL, 311:58–84, 1986 December 1

4C 29.30: EXTENDED OPTICAL LINE AND RADIO EMISSION IN A PROBABLE GALAXY MERGER

WIL J. M. VAN BREUGEL[1,2]
Radio Astronomy Laboratory, University of California, Berkeley
TIMOTHY M. HECKMAN[1,3]
Astronomy Program, University of Maryland
GEORGE K. MILEY[1,4]
Space Telescope Science Institute
AND
ALEXEI V. FILIPPENKO[2,5]
Department of Astronomy, University of California, Berkeley
Received 1985 December 6; accepted 1986 May 16

ABSTRACT

Detailed radio and optical observations of the radio galaxy 4C 29.30 provide clear morphological, polarimetric, kinematical, and energetic evidence for an interaction between the radio source and the ambient medium. *Morphology.*—The brightest optical emission-line gas is found adjacent to the most luminous radio features in the northern radio lobe, which is strongly bent "downstream" (away from the galaxy). A much fainter emission-line filament to the south roughly bounds a long ($\sim$26 kpc), straight radio jet. *Polarization.*—Regions of unpolarized radio emission are correlated with the presence of emission-line gas. *Kinematics.*—At the edges of bright radio features, the gas velocities change sharply and the emission lines become broader. The southern optical filament makes an angle of $\sim 20°$ with the radio jet, yet the jet and gas are clearly interacting; the gas velocity increases by as much as $\sim$550 km s^{-1} near the bright radio hotspot where the jet ends and decollimates. The total velocity relative to the parent galaxy is $\sim$730 km s^{-1} at the end of the filament, significantly larger than the escape velocity from the galaxy. *Energetics.*—Relative intensities of optical emission lines suggest that the gas is photoionized by a nonstellar continuum, both near the nucleus and outside it. The gas close to the nucleus is ionized by the power-law continuum detected in the nucleus itself, as in Seyfert galaxies, but this radiation is probably not strong enough to photoionize the extranuclear regions. A local mechanism plays the dominant role in the ionization of the gas, and it may be related to the presence of the radio source.

All these properties are also seen in several other objects (such as 3C 277.3) recently shown to have associated optical and radio emission, and they suggest the interaction of jets with relatively dense extranuclear gas. 4C 29.30, however, is distinguished by the optical appearance of its parent galaxy, which shows strong evidence for a previous capture of a gas-rich disk galaxy. Various "loops" or partial "shells" are visible around the object, and the central region exhibits a dust lane as well as a relatively blue secondary nucleus. We conclude that the emission lines are probably produced by the interaction of the radio source with debris from the merging process.

We hypothesize that the collision between the northern jet and a region of relatively dense gas, possibly associated with an optical shell which can be seen at this location, causes the radio emission to flare up, ionizes the gas, deflects and heats the jet material, and allows ionized gas to be mixed into the jet's boundary layers. The knotty structure in the straight southern jet, on the other hand, may be more easily understood as internal shocks in a reconfining jet as it propagates outward and adjusts to the changing pressure in the ambient medium. The sudden acceleration of the emission-line gas near the end of the jet is probably caused by a strong shock within the jet which causes it to rapidly expand and decollimate.

From the [S II] $\lambda\lambda$6716, 6731 doublet we estimate the gas density in the emission-line regions. It is shown that the total amount of gas in the northern lobe may indeed be sufficient to have deflected the jet, and that the thermal gas and radio-emitting plasma may be in pressure equilibrium, as in some other radio galaxies with optical emission-line regions. The latter result helps validate (to within an order of magnitude) the many ad hoc assumptions that are generally made to estimate the pressure in radio-emitting plasmas.

We stress that the observed gas velocities are not those of the jet material itself, but are related to the velocities of expansion and translation at the boundaries (cocoons, lobes) of the radio source as it heats and

[1] Visiting Astronomer at the Very Large Array of the National Radio Astronomy Observatory, at Kitt Peak National Observatory of the National Optical Astronomy Observatories, and at Steward Observatory of the University of Arizona.
[2] Visiting Astronomer at Lick Observatory, University of California.
[3] Alfred P. Sloan Fellow.
[4] On leave from Leiden Observatory, The Netherlands.
[5] Miller Research Fellow.

accelerates the ambient gas. Likewise, the low radio polarization near regions of emission-line gas is probably not caused by dense ionized gas internal to the jet, but instead may be due to "Faraday screens" produced by ionized clumpy material entrained in the outer layers of the radio source. Moreover, the radio emission represents only a small fraction of the total energy in the jets powering the radio source. We estimate that the total luminosity of the emission lines in the northern lobe is at least 10 times that at radio wavelengths; the jet therefore converts $\lesssim 10\%$ of its energy into radio synchrotron emission. Most of the energy is apparently used to heat and accelerate the ambient gas. The observed properties of 4C 29.30, such as the large misalignment between the emission-line filament and the southern radio jet, emphasize that radio galaxies need to be studied with a variety of techniques to sample the rich spectrum of physical processes that can be involved in the interactions of extragalactic jets with their environment.

Subject headings: galaxies: individual — galaxies: internal motions — galaxies: jets — galaxies: structure — polarization — radio sources: galaxies

I. INTRODUCTION

Observations of radio galaxies with extended optical emission-line gas are changing our perspective on extragalactic radio sources and their environment. They are showing that the interaction of radio jets and lobes with relatively dense ambient gas is important in many radio sources (see, for example, van Breugel and Heckman 1982; Miley 1983; van Breugel 1986). Collisions of jets with dense material may deflect and disrupt the jets, and optical synchrotron emission associated with internal shocks may photoionize the surrounding gas, as in 3C 277.3 (Miley *et al.* 1981; van Breugel *et al.* 1985*a*). In other situations, jet-induced star formation may occur; excellent examples are Centaurus A (see, e.g., Graham and Price 1981) and "Minkowski's Object" (van Breugel *et al.* 1985*b*). Entrainment of ionized ambient gas in the turbulent boundaries of the sources may depolarize the radio emission, as in 3C 305 (Heckman *et al.* 1982), 4C 26.42 (van Breugel, Heckman, and Miley 1984), and 3C 277.3 (van Breugel *et al.* 1985*a*). The entrained gas may be transported over many kiloparsecs, to be deposited in distant radio lobes (3C 277.3).

During the course of our continuing study of radio galaxies, we have discovered extended optical line emission associated with 4C 29.30 (0836+299; $z = 0.0643$; $m_{pg} = 15.7$; see Table 1). The emission-line region is among the most extended we have found; its observed angular size ($\sim 40''$) translates into a projected length of ~ 45 kpc, under the assumptions $q_0 = 0.5$ and $H_0 = 75$ km s^{-1} Mpc^{-1} (used throughout this paper). The data support the general picture of jet and gas interactions described above. They also provide a clue to the origin of the extranuclear gas, which is often unclear in other cases: the parent galaxy of 4C 29.30 appears to have merged with a gas-rich (disk) galaxy. In addition, both the energetics and morphology of the emission-like gas show that the radio emission represents only a small fraction of the energy outflow from the nucleus of 4C 29.30.

TABLE 1

GLOBAL PROPERTIES OF 4C 29.30 (0836+299)[a]

Radio	
Flux density (1415 MHz)	0.70 Jy[b]
Monochromatic power (1415) MHz)	5.7×10^{31} ergs s^{-1} Hz^{-1}
Total radio luminosity	9.1×10^{41} ergs s^{-1}
Spectral index $\alpha (S_\nu \propto \nu^{-\alpha})$	0.65[b]
Optical	
Redshift	0.0643[c]
Luminosity distance	261 Mpc
Linear/angular scale ratio	1.12 kpc arcsec^{-1}
Absolute visual magnitude	−22.3

[a] $H_0 = 75$ km s^{-1} Mpc^{-1}; $q_0 = 0.5$.
[b] Colla *et al.* 1975; 1 Jy = 10^{-23} ergs s^{-1} cm^{-2} Hz^{-1}.
[c] Measured from emission lines in nucleus.

II. OBSERVATIONS AND REDUCTIONS

Radio and optical data were obtained at several observatories, as summarized in Tables 2 and 3. Standard procedures (e.g., van Breugel *et al.* 1985*a*) were followed for their calibration and analysis, and are only briefly described here.

a) Radio Imaging

4C 29.30 was observed with the Very Large Array (VLA) in the A-, B-, and C-array configurations (Thompson *et al.* 1980) at wavelengths of 20.6 cm, 6.2 cm, and 2.0 cm, respectively. This allowed comparison of three different high-resolution maps ($1\farcs3$) with comparable sampling of the radio source structure. The source was also observed at 6.2 cm in the A-array, yielding maps with even higher resolution ($0\farcs3$), and at 20.6 cm in the B-array, providing better sensitivity to extended structure of low surface brightness.

b) Optical Imaging

We used the video camera (Robinson *et al.* 1979) on the 2.1 m telescope and a prime focus Fairchild CCD (PFCCD; Marcus, Nelson, and Lynds 1979) on the 4 m Mayall telescope of Kitt Peak National Observatory (KPNO) to obtain broad-band and narrow-band images of the parent galaxy of 4C 29.30. The video camera and PFCCD observations, together with subsequent processing, were similar to those described in Heckman (1981) and van Breugel *et al.* (1985*a*). The narrow-band images were placed on an absolute flux scale with observations of standard stars.

c) Slit Spectroscopy

Observations through a long slit were made at KPNO on the 4 m telescope with the high gain video spectrometer (HGVS; see, e.g., Ford 1979) and the cryogenic camera (De Veny 1983), and at Lick Observatory on the 3 m Shane telescope with the new Cassegrain CCD spectrograph (Miller 1983). The slits were positioned along the major extensions of the central and northern emission-line regions, at position angles (P.A.) of 4° and 95°, respectively. With the cryogenic camera a spectrum was also obtained at P.A. = 85° through the nucleus.

The CCD-based cryogenic camera is more sensitive than the HGVS, except at wavelengths below ~ 4500 Å. These observations were aimed at studying spatial variations in the emission-line intensity ratios and the overall kinematics of the gas. The

TABLE 2

JOURNAL OF RADIO (VLA) OBSERVATIONS

VLA Configuration	Observing Date	Frequency (MHz)	Wavelength (cm)	Bandwidth (MHz)	Resolution	Observing Time (hr)
A.....	1982 Feb	4873	6.2	25	0".3 × 0".3	4
A.....	1982 Feb	1452	20.6	25	1.3 × 1.3	4
B.....	1981 Jul	4873	6.2	25	1.3 × 1.3	6
B.....	1981 Jul	1452	20.6	25	4.5 × 4.5	2
C.....	1981 Oct	14965	2.0	50	1.3 × 1.3	12

HGVS, on the other hand, has better spectral resolution (~4.2 Å rather than ~15 Å), so [O III] λ5007 was used to study in detail the kinematics of bright emission-line regions. Finally, the Lick CCD spectrograph is more sensitive than the HGVS in the red part of the spectrum, and its resolution (~7 Å) is sufficient to resolve the (Hα + [N II]) complex and the [S II] λλ6716, 6731 doublet. This allowed us to determine the velocity gradient along the faint southern filament and to estimate the density of the emission-line gas at various locations.

Observation and reduction procedures were similar to those described by Heckman *et al.* (1981). The KPNO long-slit spectra were corrected for variations in detector response along the slit direction, but not along the dispersion. Thus, relative line intensities [i.e., $H\alpha/H\beta \equiv I(H\alpha)/I(H\beta)$] could not be reliably obtained from these data, but spatial differences in such ratios along the slit, as well as the kinematics of the gas, could nevertheless be extracted. The long-slit Lick spectra were obtained under photometric conditions and 1" seeing and were calibrated on an absolute flux scale with standard stars.

d) Aperture Spectroscopy

Dual-aperture observations were made at the Multiple Mirror Telescope (MMT) with the photon-counting intensified Reticon spectrograph (IRet; Shectman 1981), and at Lick with the image-tube scanner (ITS; Miller, Robinson, and Wampler 1976), to obtain additional information about the intensity ratios in the nucleus and in the northern emission-line regions of 4C 29.30. The Lick observations were specifically designed to record the blue part of the spectrum, in which several important high-excitation lines and a nonstellar continuum might be visible. They were photometrically calibrated with standard stars, whereas the MMT spectra were not.

III. RESULTS

a) Identification of 4C 29.30

Some confusion in the literature exists concerning the identification of 4C 29.30 because two different radio galaxies have been labeled "0836+29." Their more accurate "coordinate" designations would be 0836+290 and 0836+299. The former is identified with a cD galaxy in the cluster Abell 690 (Owen, Rudnick, and Peterson 1977; Fanti *et al.* 1977), while 0836+299 is 4C 29.30 (Colla *et al.* 1975). As a result of this confusion, 0836+290 in Abell 690 was assigned the wrong redshift by Owen, Rudnick, and Peterson (1977); 4C 29.30 ($z = 0.0643$) is probably not a member of this cluster ($z = 0.0790$). Inspection of the Palomar Sky Survey plates shows that there are several fainter galaxies within ~30′, so 4C 29.30 may nevertheless be the brightest member of a small cluster or group.

The optical position of the center of the galaxy [$\alpha(1950) = 08^h36^m59^s.0 \pm 0^s.4$, $\delta(1950) = 29°59'43".5 \pm 0".8$] was measured from the Palomar Sky Survey plates with the Grant measuring machine at KPNO and is indicated in Figure 1. We identify the radio component C2 (Table 4) with the nucleus because of its flat radio spectrum, compactness, and agreement in position. When aligning our optical images with the radio maps, we therefore assumed that this component coincides with the optical nucleus.

b) Radio Emission

i) *Morphology*

The large-scale and small-scale radio structures of 4C 29.30 are shown in Figure 1 ($\lambda = 21$ cm, 1".3 resolution), Figures 2 and 3 (6 cm, 0".3), and Figure 4 (21 cm, 4".5). These maps were

TABLE 3

JOURNAL OF OPTICAL OBSERVATIONS

Parameter	Optical Image	Optical Image	Slit Spectrum	Slit Spectrum	Slit Spectrum	Aperture Spectrum	Aperture Spectrum
Telescope	KPNO 4 m	KPNO 2.1 m	KPNO 4 m	KPNO 4 m	Lick 3 m	MMT	Lick 3 m
Instrument	Prime focus CCD	Video camera	HGVS	Cryogenic camera	Cassegrain CCD	IRet	Cassegrain ITS
Angular resolution	1" FWHM	1".5 FWHM	1"	1"	1"	...	...
Field size (or aperture) ...	85" × 112"	130" × 130"	2".5 × 166"	2".5 × 248"	2".2 × 130"	1".8 × 2".9	4" × 4"
Position angle	...	...	4°; 95°	85°; 85°	4°; 95°	...	...
Location (with respect to nucleus)	...	...	At nucleus; 3"E, 11"N	At nucleus; 3"E, 11"N	At nucleus; 3"E, 11"N	3"E, 11"N	At nucleus
Spectral resolution	...	...	4.2 Å	15–20 Å	7 Å	6 Å	10 Å
Δλ band	Red: 1400 Å Hα: 75 Å	Hα: 75 Å [O III]: 55 Å	5100–5800 Å	4600–8000 Å	5800–8000 Å	4200–7700 Å	3190–7070 Å
Date	1982 Jan	1981 Jan	1982 Apr	1981 Oct	1985 Jan	1981 Nov	1985 Jan–Mar
Purpose	Optical structure of galaxy and emission-line regions		Kinematics	Ionization state	Kinematics; gas density	Ionization state	Ionization state; continuum

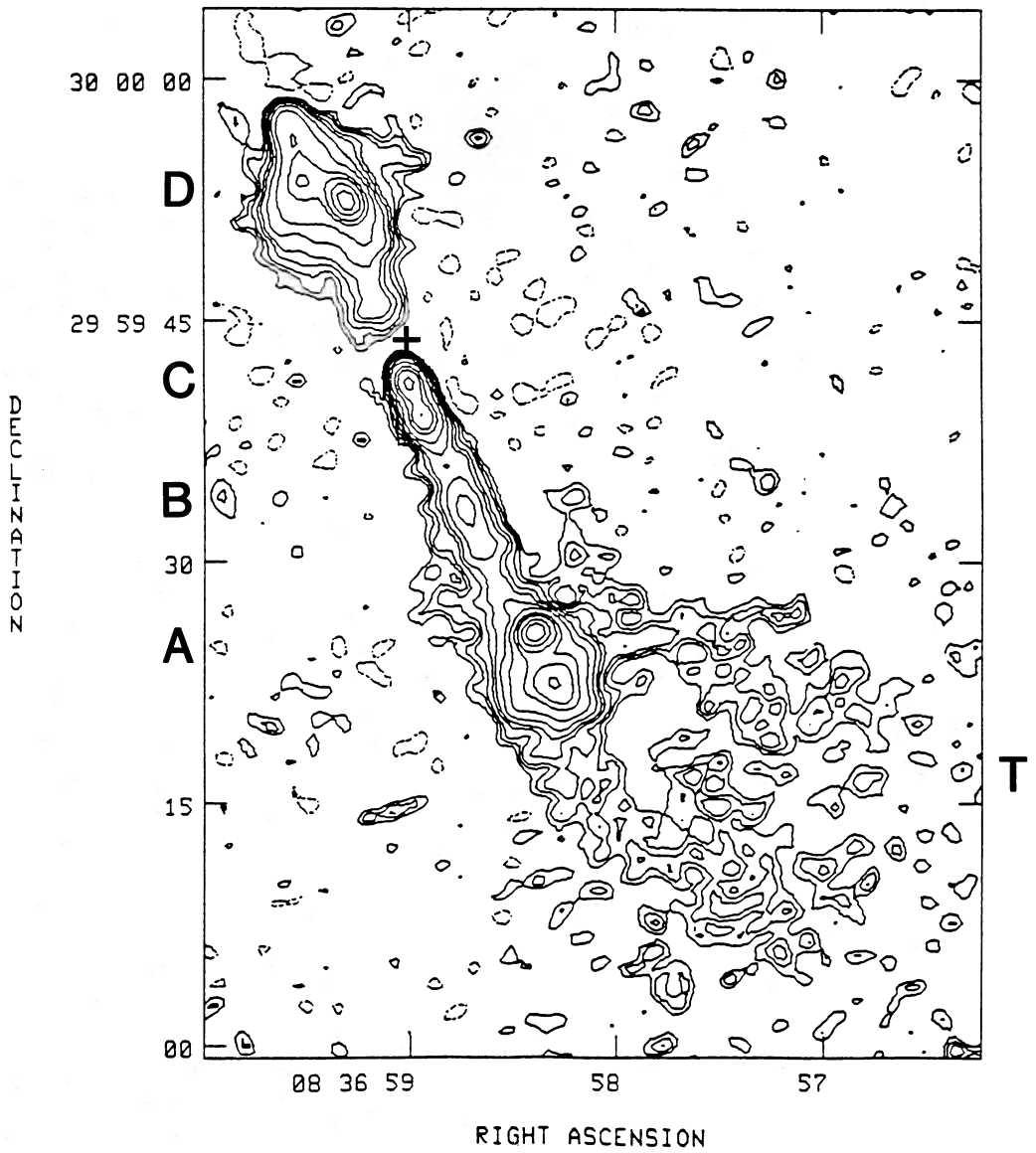

FIG. 1.—Contour representation of the total intensity of 4C 29.30 at $\lambda = 20.6$ cm (1".3 × 1".3 resolution). Various features referred to in the text are labeled: the tail T, the southern lobe A, and the jet B, the core C, and the northern lobe D. Contour values (mJy beam^{-1}) are $0.15 \times (-2, 2, 3, 4, 6, 8, 12, 20, 40, 60, 100,$ and 150). Negative values appear as dashed lines. The cross indicates the optical position of the galactic nucleus.

made with the combined A- and B-arrays. At 2 cm only the brightest components were detected, and no map is shown. We note the following.

1. The radio source is asymmetrical: the "arrow shaped" northern lobe (D) is relatively compact and close to the nucleus, while the southern part contains a long jet (B, C) and a diffuse tail (T) which appears swept back to the west. In general, the steepest intensity gradients seem to be at the northeastern sides.

2. The long and knotty jet (B) extends southwest from the nucleus and ends at a bright knot (A2) in the southwest lobe (A). The bright region near the nucleus is double (C1, C2) and exhibits a small wiggle. Its overall size (~3 kpc), spectral index between 6 cm and 21 cm ($\alpha_6^{21} = 0.7$ for the combined components, where $S_\nu \propto \nu^{-\alpha}$), and morphology resemble those of objects with "steep-spectrum radio cores," which are often found embedded in Seyfert galaxies, peculiar gas-rich elliptical galaxies, and certain quasars (van Breugel, Miley, and Heckman 1984).

3. The increasing widths of the jet's components C1, B, and A2 indicate that the jet expands slowly. The faintness of the major portion of the jet (component B, which is resolved at 6 cm in the A-array) precludes an accurate measurement of the expansion rate as a function of distance from the nucleus.

4. South of knot A2, lobe A flares out and merges with the diffuse tail T. This region appears edge brightened, and may be another example of "radio shells" or "bubbles" such as those found in NGC 3079 (Duric *et al.* 1983), 3C 310 (van Breugel and Fomalont 1984), and 3C 348 (Dreher and Feigelson 1984).

5. The radio knots, when observed with 1".3 resolution (Fig. 1), seem to come in pairs. We find that (*a*) the brightest knot is always closest to the nucleus and has its steepest intensity gradient on that side; (*b*) the brightness ratios of the knots in each pair are similar (~2:1); and (*c*) the separation between

TABLE 4A

OBSERVATIONAL PARAMETERS OF THE RADIO EMISSION

Component (1)	Angular Size (2)	Flux Density (mJy) (3)	Spectral Index α_6^{21} (4)	Percent Pol. (P) at 6 cm (5)	Depolarization $(DP)_6^{21}$ (6)	Faraday Rotation $(\Delta\phi)_6^{21}$ (7)
			$\lambda = 6$ cm			
A1	2".5 × 2".5	~19	0.82 ± 0.05	11 ± 2	1.0 ± 0.2	60 ± 5
A2	0.6 × 1.2	~15	0.80 ± 0.05	36 ± 1	1.0 ± 0.1	65 ± 5
C1	0.67 × 0.25[a]	6.1 ± 0.4	0.86 ± 0.05	<4 (3σ)	...	...
C2	<0.45 × 0.45	10.4 ± 1.3	0.22 ± 0.05	<2 (3σ)	...	...
D1	0.48 × 0.44[b]	8.1 ± 0.8	0.88 ± 0.05	9 ± 1	1.0 ± 0.1	65 ± 10
D2	0.76 × 0.43[c]	8.1 ± 1.0				
D3	~1.0 × 2.2	6	0.80 ± 0.05	28 ± 3	...	60 ± 5
			$\lambda = 21$ cm			
A.....	5".3 × 6".5	154	...	...	...	...
B.....	1 × 12	32	0.92 ± 0.10	<13[d]	...	...
C	0.45 × 3	51	...	...	...	...
D	5.7 × 11	161	...	...	...	...
T.....	40 × 40	260	...	...	...	...
TS[e]	40 × 80	658	...	...	...	...

NOTES.—Col. (1): See Figs. 1, 2, and 3 for identifications of components; cols. (4), (6), and (7): Determined from the 1".3 × 1".3 resolution maps.

[a] P.A. = 14°.

[b] P.A. = 133°.

[c] P.A. = 29°.

[d] Polarization measurement (3 σ upper limit) of component B at $\lambda = 6$ cm.

[e] TS = total source.

TABLE 4B

PHYSICAL PARAMETERS OF THE RADIO EMISSION

Component (1)	Total Radio Luminosity (10^{40} ergs s^{-1}) (2)	Assumed Path Length (kpc) (3)	Magnetic Field Strength (10^{-4} G) (4)	Equivalent Thermal Pressure (10^6 K cm^{-3}) (5)	Minimum Total Energy (10^{55} ergs s^{-1}) (6)	Radiative Lifetime at 6 cm (10^6 yr) (7)
A1	6	2.8	0.5	1	16	1
A2	5	1.3	1.1	5	4	0.3
C1	2	0.3	2.1	20	0.7	0.1
C2	...	<0.5	...	...	...	...
D1	2.5	0.5	1.9	16	1.3	0.1
D2	2.5	0.5	1.7	13	1.6	0.2
D3	2	2.4	0.5	1	4.6	1
A.....	20	7	0.3	0.4	78	2
B.....	4	13	0.2	0.2	22	4
C	...	<0.5	>1	>8	>4	<0.2
D	21	6	0.3	0.4	124	2
T.....	34	44	0.086	0.03	16000	13

NOTES.—Col. (1): See Figs. 1, 2, and 3 for identifications of components; cols. (2)–(7): Subject to various assumptions (see § III*b*).

knots increases slightly (from 2.6 kpc to 3.7 kpc) with increasing distance from the nucleus.

ii) *Polarization*

The polarization distributions of 4C 29.30 (percentages P, and position angles P.A.) at 6 cm and 21 cm are shown in Figures 5*a* and 5*b*. At 2 cm the signal-to-noise (S/N) ratio is rather poor, and polarization is only detected from the central region of component A2: $P = 34\% \pm 6\%$, with P.A. = 37° ± 5°. We can place 3 σ upper limits of $P \approx 14\%$ to C2, D1, and D2, and of $P \approx 40\%$ to A1, C1, and D3. No polarization is detected from the jet at any of the three wavelengths. The most useful upper limits are obtained at 6 cm (Table 4).

At the other locations the percentage polarization appears highest near steep gradients in the total intensity, as is usually observed in radio galaxies. The values (at 6 cm) range from 9% ± 1% in the northern lobe (D1, D2), to 36% ± 1% in the southern lobe (A2). At 21 cm the tail (T) is ~30% polarized (at 4".5 resolution), but the uncertainties are large (~15%) because of its low surface brightness.

iii) *Spectral Comparisons and Physical Parameters*

We have compared the 1".3 resolution maps at the three wavelengths, using matched visibility data from the three array configurations, to determine the spectral index α, the polarization rotation ($\Delta\phi$, defined as the difference between the polarization position angles, P.A.(λ_1) − P.A.(λ_2), with $\lambda_1 > \lambda_2$),

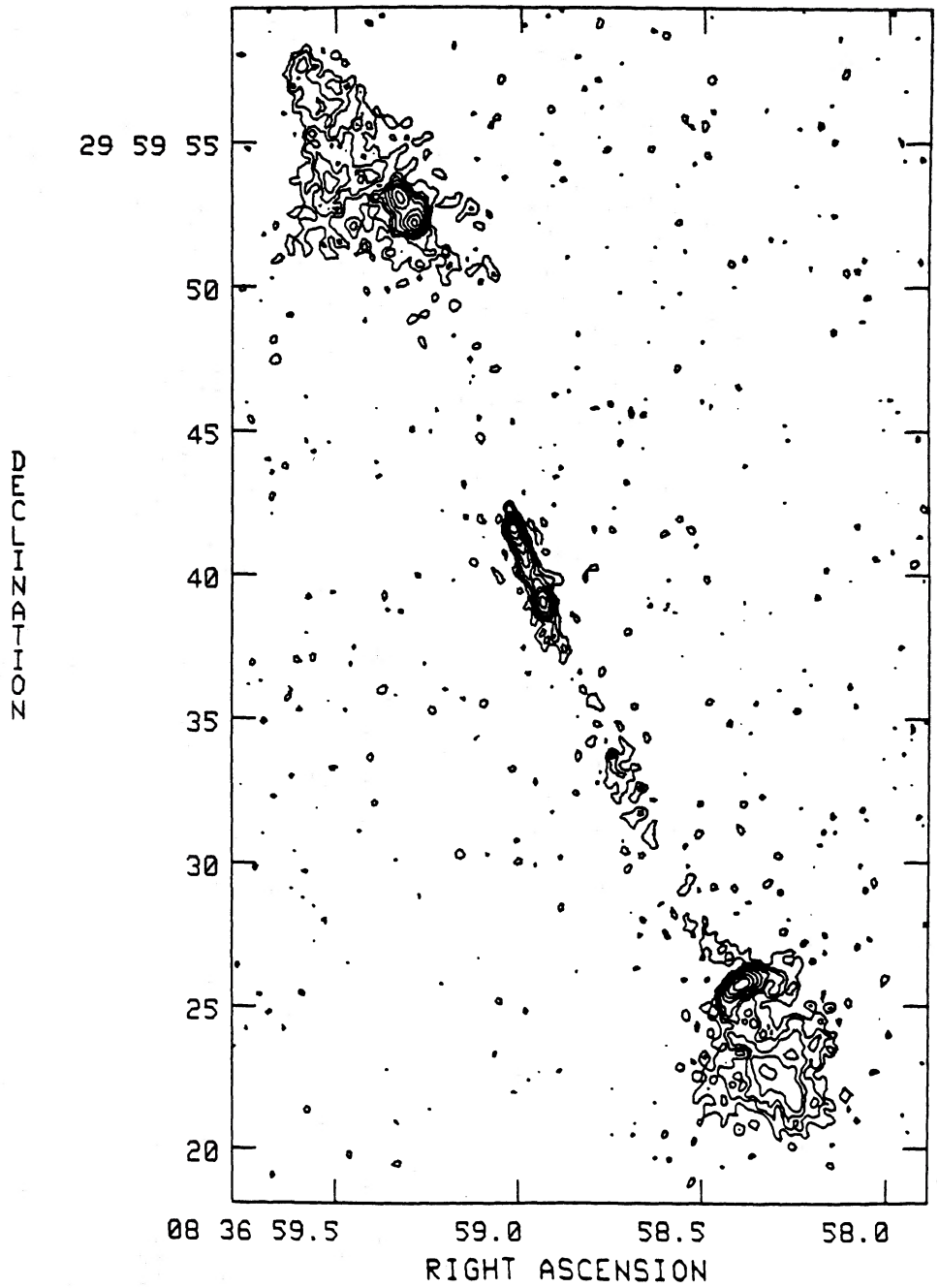

FIG. 2.—Contour representation of the total intensity of 4C 29.30 at $\lambda = 6.2$ cm (0".3 × 0".3 resolution). Various features referred to in the text are labeled; see also Fig. 1. Contour values (mJy beam^{-1}) are 0.05 × (−3, 3, 5, 7, 10, 16, 25, 40, 60, and 100). Negative values appear as dashed lines.

and the depolarization (DP, defined as the ratio of the percentage polarization $P(\lambda_1)/P(\lambda_2)$, with $\lambda_1 > \lambda_2$). The results for the comparison of the 6 cm and 21 cm maps are summarized in Table 4.

Despite the mediocre S/N ratio at $\lambda = 2$ cm, the α_2^6 spectral indices are consistent with the α_6^{21} values. Polarized emission is detected only from component A2, as mentioned above, and we find no significant depolarization or rotation in this region: $(DP)_2^6 = 0.9 \pm 0.2$ and $(\Delta\phi)_2^6 = 3° \pm 7°$.

We have also compared the low resolution (4".5) maps at 6 cm and 21 cm. This gave results which are in agreement with those obtained at 1".3 resolution.

The radio spectral properties are similar for the various components in 4C 29.30:

1. Except for the nucleus (C2), the spectral index is comparable at all locations in the source, irrespective of distance from the nucleus. On average, $\alpha_6^{21} = 0.85$, which is somewhat larger than the spectral index at lower frequencies for the entire source ($\alpha = 0.71$; Colla *et al.* 1975).

2. $(DP)_6^{21} \approx 1$ in all of the components where polarization at two wavelengths is detected.

3. The rotation of the polarization position angles between 6 cm and 21 cm is constant across the source ($\sim +60°$).

Using the standard minimum-energy arguments as in our

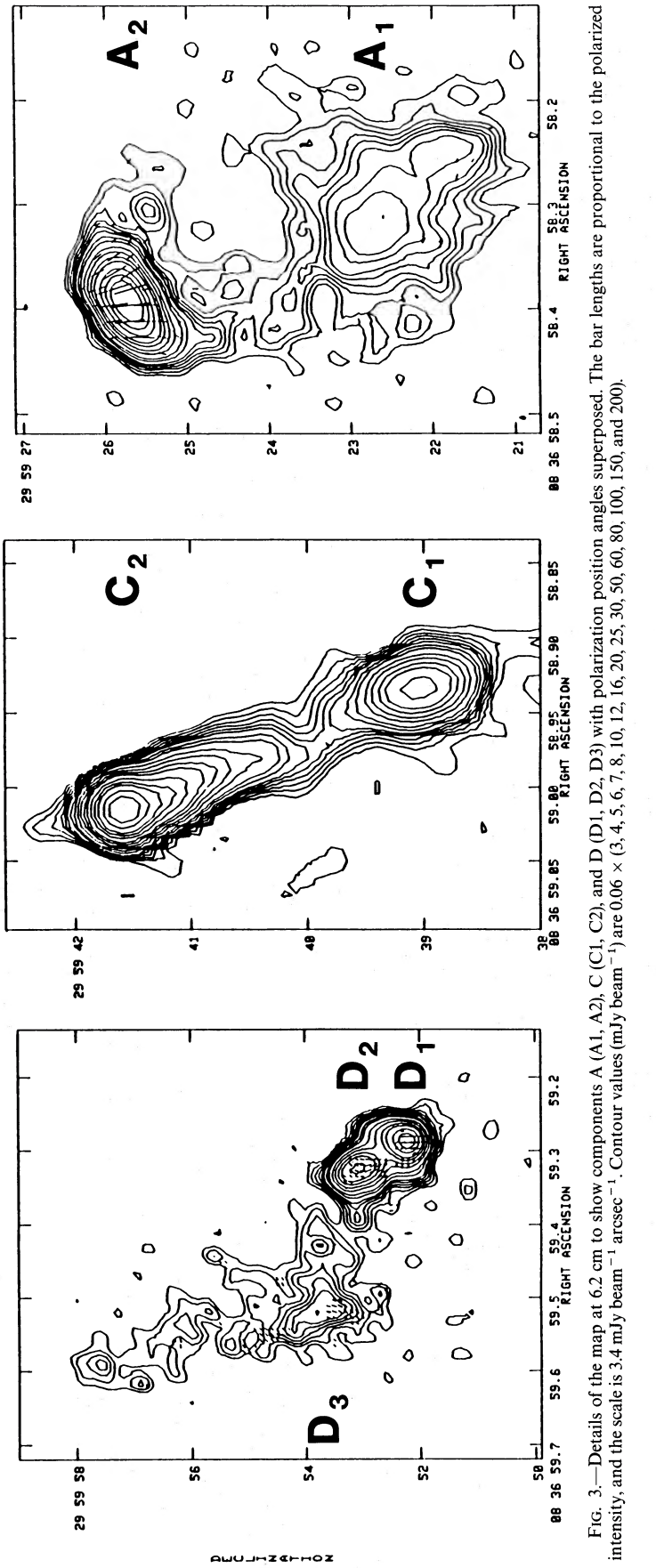

FIG. 3.—Details of the map at 6.2 cm to show components A (A1, A2), C (C1, C2), and D (D1, D2, D3) with polarization position angles superposed. The bar lengths are proportional to the polarized intensity, and the scale is 3.4 mJy beam^{-1} arcsec^{-1}. Contour values (mJy beam^{-1}) are $0.06 \times (3, 4, 5, 6, 7, 8, 10, 12, 16, 20, 25, 30, 50, 60, 80, 100, 150, \text{and } 200)$.

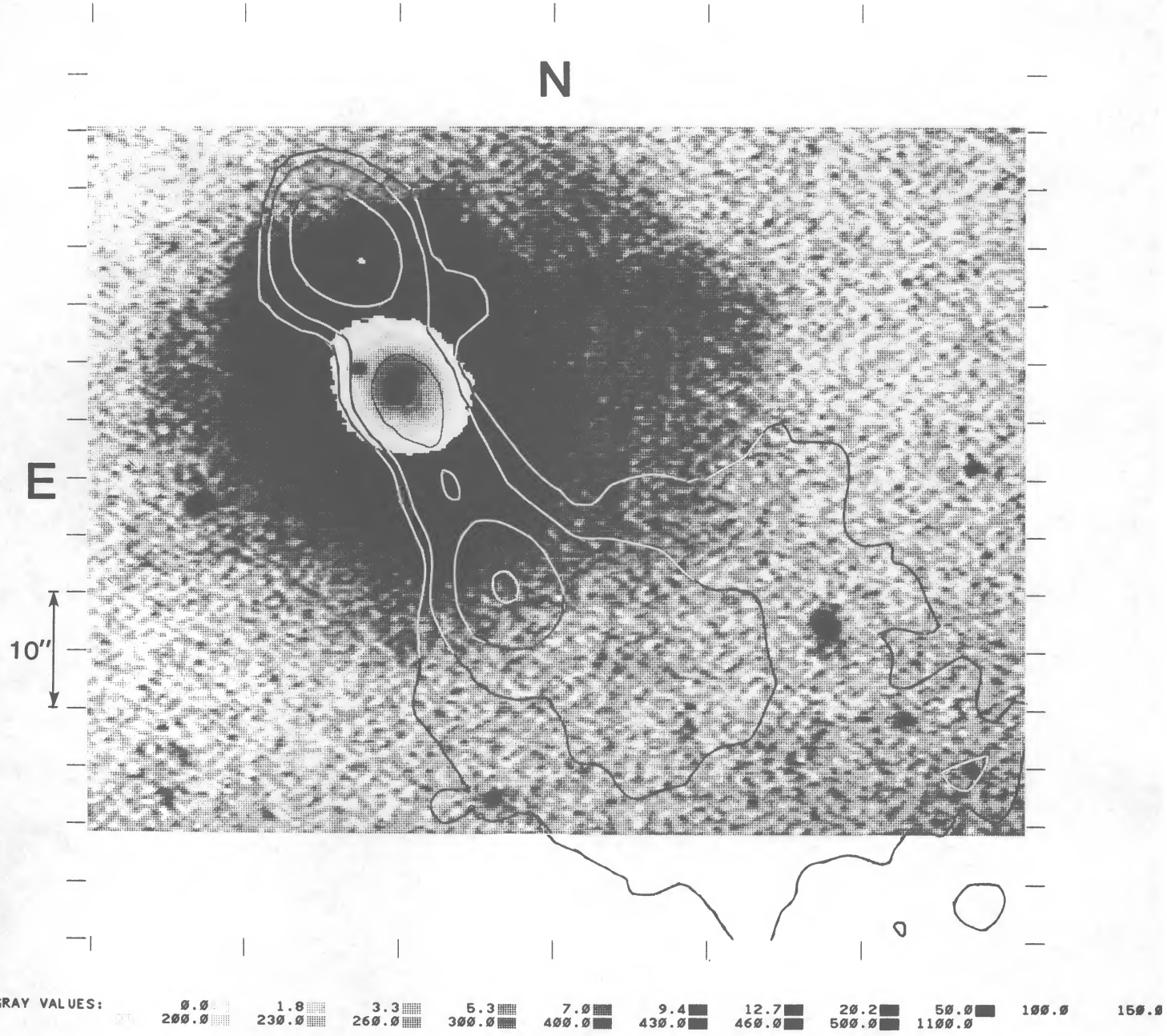

FIG. 4.—Contour representation of the total intensity of 4C 29.30 at 20.6 cm (4″.5 × 4″.5 resolution), superposed on a gray-scale reproduction of a red PFCCD image. Contour values (mJy beam^{-1}) are 1.0, 1.9, 7.7, and 34.6.

previous papers (e.g., Miley 1983), we have derived various physical parameters for the radio-emitting plasma, as listed in Table 4. Only marginally lower values would be found if one were to use minimum-pressure arguments (Burns, Owen, and Rudnick 1979; Killeen, Bicknell, and Ekers 1986).

c) Optical Emission

i) *Morphology: Comparison with Radio Maps*

The broad-band red PFCCD image of 4C 29.30, overlaid with a low-resolution radio map, is shown in Figure 4. Photographic reproductions are shown in Figures 6*a*, 6*b*, and 6*c* (Plates 3 to 5). These images indicate that

1. The galaxy is peculiar, exhibiting faint loops and arcs (Figs. 6*a* and 6*b*) that resemble the "shells" seen in certain nearby elliptical galaxies (Malin and Carter 1983).

2. A dust lane seems to be present in the nuclear region (Fig. 6*c*). The major axis of the source is at a large angle with respect to this lane (compare Figs. 1 and 6*c*), as is often the case in other objects (Kotanyi and Ekers 1979).

3. Northeast of the main nuclear region is a compact feature which may be a secondary nucleus, but a measurement of its redshift is necessary to verify this. It is $\sim$0.5 magnitude bluer than the primary nucleus, as derived from our continuum narrow-band images taken with the video camera.

4. The brightest parts of the radio source are embedded within the galaxy, whereas the radio tail appears to be outside the main body.

The narrow-band (Hα + [N II]) PFCCD image of 4C 29.30 is shown in Figures 7*a* and 7*b*, overlaid with a 0″.3 resolution map made at 6 cm and a 4″.5 resolution map made at 21 cm,

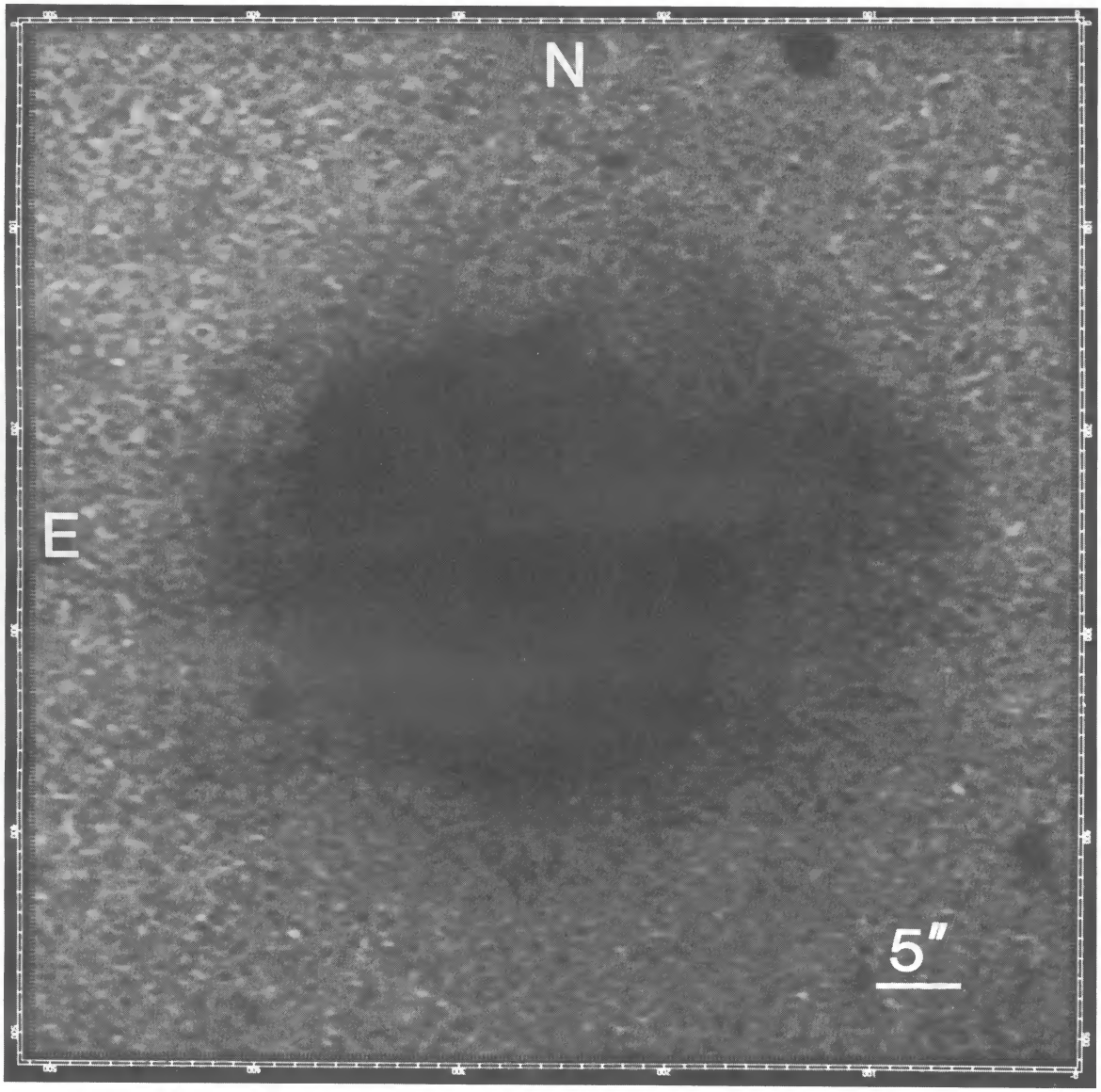

FIG. 6*a*

FIG. 6.—Photographic reproductions of the broad-band red PFCCD image. The asymmetric structure of the galaxy and the faint "loops" and partial "shells" are shown in (*a*) and (*b*); also note the sharp northeastern edge in (*b*). The nuclear region, with the dust lane and the secondary nucleus to the northeast, is illustrated better in (*c*). {Hα + [N II] $\lambda\lambda$6548, 6583} line emission is included in the red bandpass, which results in some confusion with the continuum in the central and northern regions.

PLATE 4

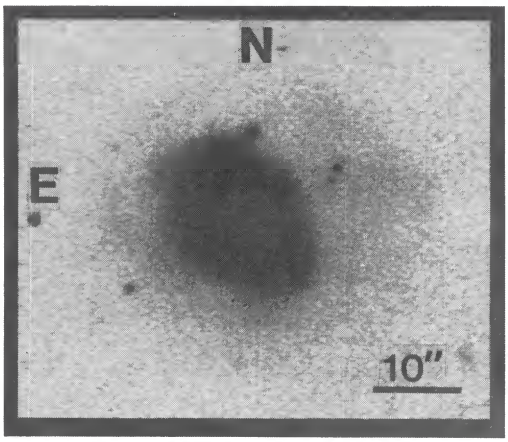

FIG. 6*b*

VAN BREUGEL *et al.* (*see* page 65)

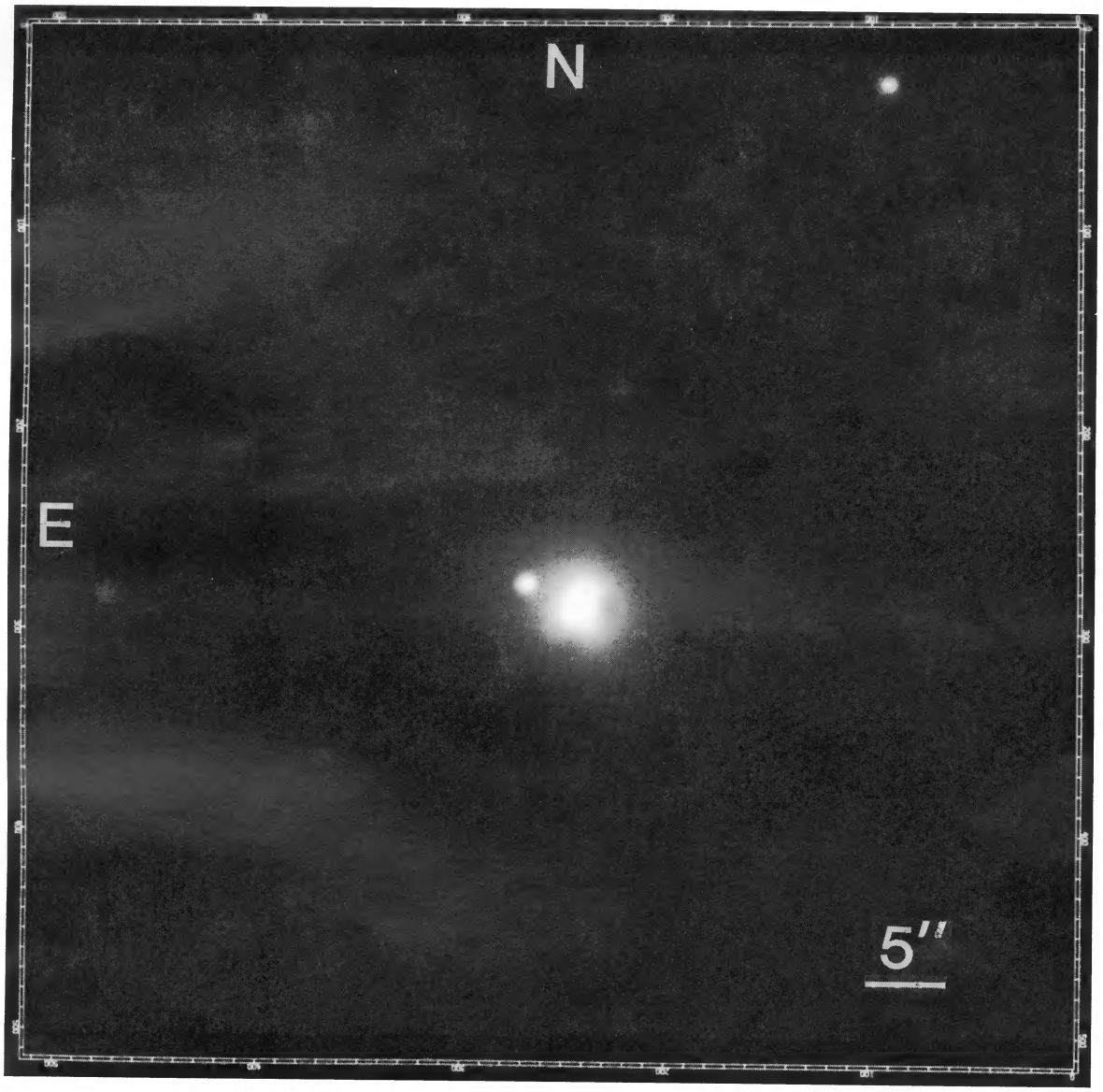

FIG. 6*c*

VAN BREUGEL *et al.* (*see* page 65)

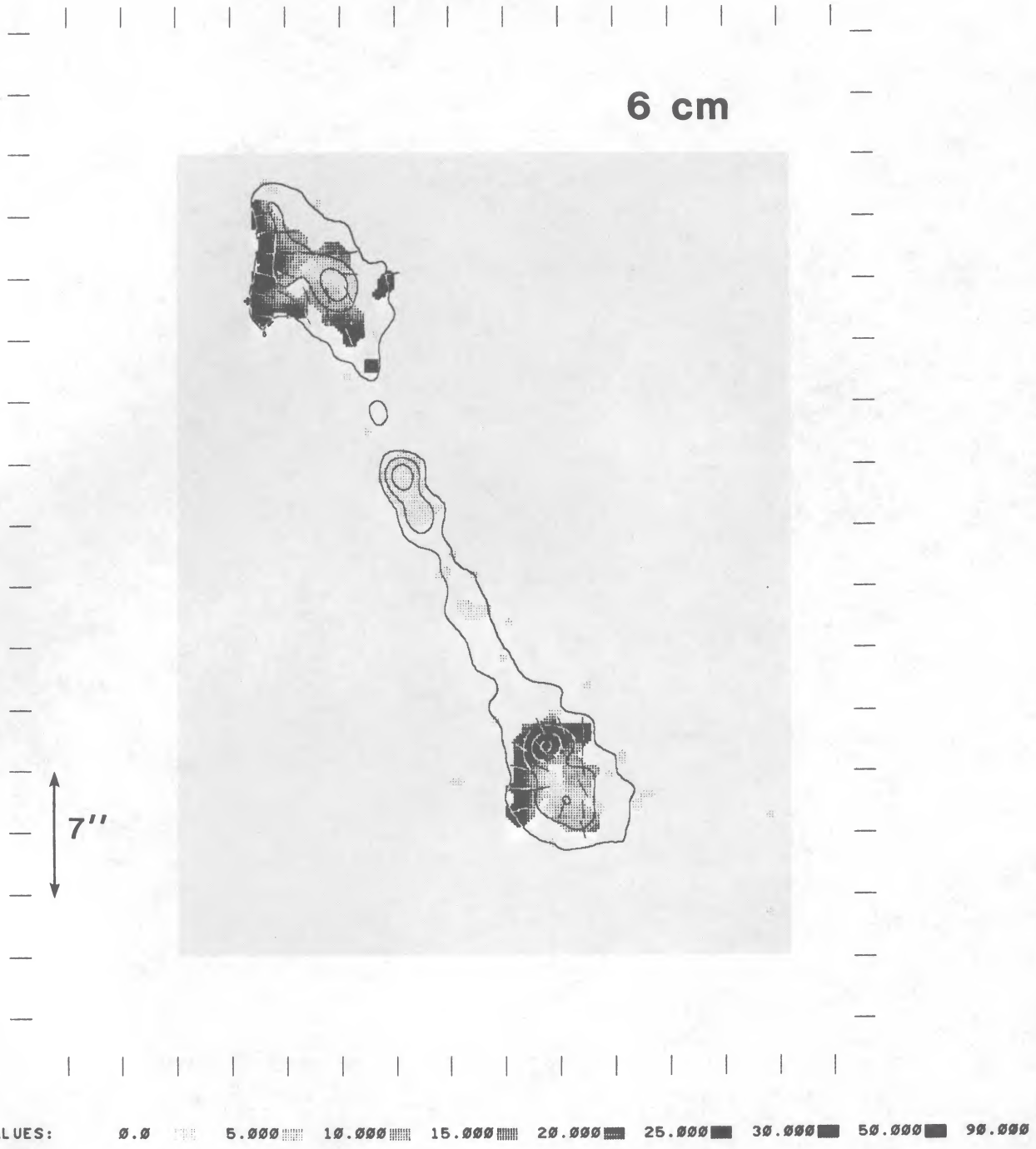

FIG. 5*a*

FIG. 5.—Gray-scale representation of the percentage polarization (values as shown at the bottom), with polarization position angles superposed (arbitrary bar lengths), at (*a*) $\lambda = 6.2$ cm and (*b*) $\lambda = 20.6$ cm. The resolution is $1''.3 \times 1''.3$. Contour values of the total intensity (mJy beam^{-1}) are 0.06, 2.4, 6, 11 (at 6.2 cm), and 1.7, 7, 17, 30 (at 20.6 cm). Gray values correspond to the percentage of polarized intensity (as indicated).

respectively. Individual emission-line regions are indicated. In Figure 8 we present the video camera images of the (Hα + [N II]) and the [O III] λ5007 emission, superposed on maps of the total and polarized intensity at 6 cm. Small discrepancies in the video camera and PFCCD images may be due to differences in sensitivity (worse in the red region for the video camera), the off-band continuum subtraction, and the atmospheric seeing. In general, however, the images agree rather well and show the amazing complexity of the optical emission-line regions in 4C 29.30. There are two northern emission-line regions (one of which appears "hooked"; Fig. 7*a*), a slightly "Z-shaped" nuclear region with evidence for an emission-line "ring" or "disk" (best seen in the [O III] Video Camera image, Figs. 8*c*, *d*), and a faint, long filament to the south (Fig. 7*a*). Comparison of the central region with the broad-band red PFCCD image suggests that the dust lane might exhibit optical line emission.

There is much evidence that the optical line and radio continuum emission are related.

1. The total extent of the optical line emission is 40″ (~45

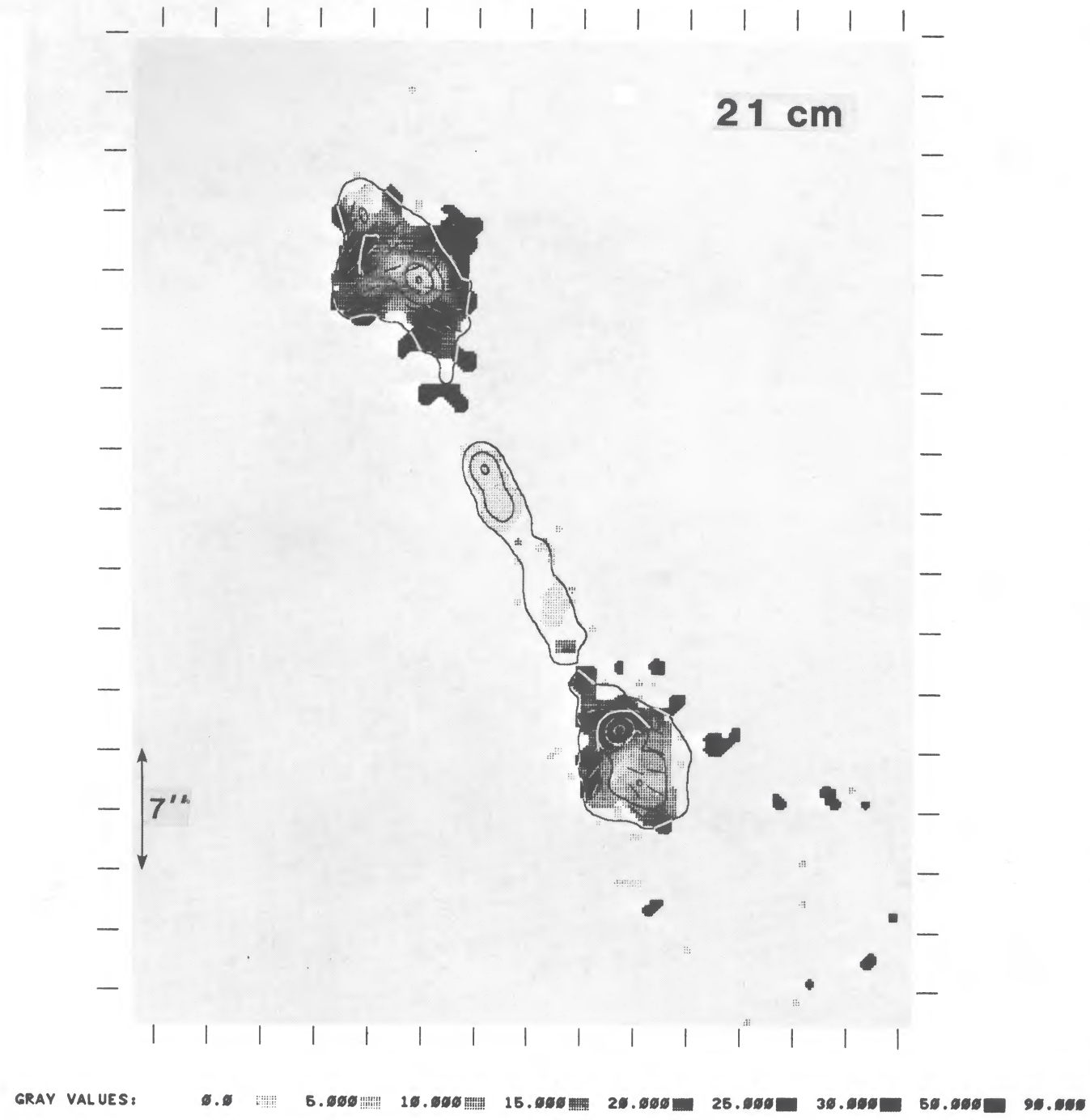

FIG. 5*b*

kpc projected length), comparable to that of the bright radio emission within the galaxy.

2. Outside the nuclear region, the line emission is brightest near the northern lobe (NL1, NL2). The location of maximum emission-line brightness is slightly offset (Fig. 8) from the radio continuum knots D1 and D2. An additional brightness enhancement both at radio and optical wavelengths occurs near D3, where the radio and optical emission are again offset.

3. The optical filament (F) and the radio jet south of the nuclear emission-line region are misaligned by $\sim 20°$. There is only marginal evidence for weak radio emission between these features (compare Figs. 1 and 7*b*). It should be noted that the exact coincidence of the emission-line filament with the boundaries of the radio emission in Figure 7*b* is only suggestive, since the resolution of the radio map is quite low. Despite this misalignment, the kinematics of the gas (see § III*c*(ii) below) strongly implies that it is influenced by the radio jet.

4. The source is unpolarized at both 6 cm and 21 cm close to regions where bright optical and radio emission overlap, e.g., near the inner jet (C1, C2) and knots D1, D2. A little polarization is detected near the latter, at the edges of the emission-line region.

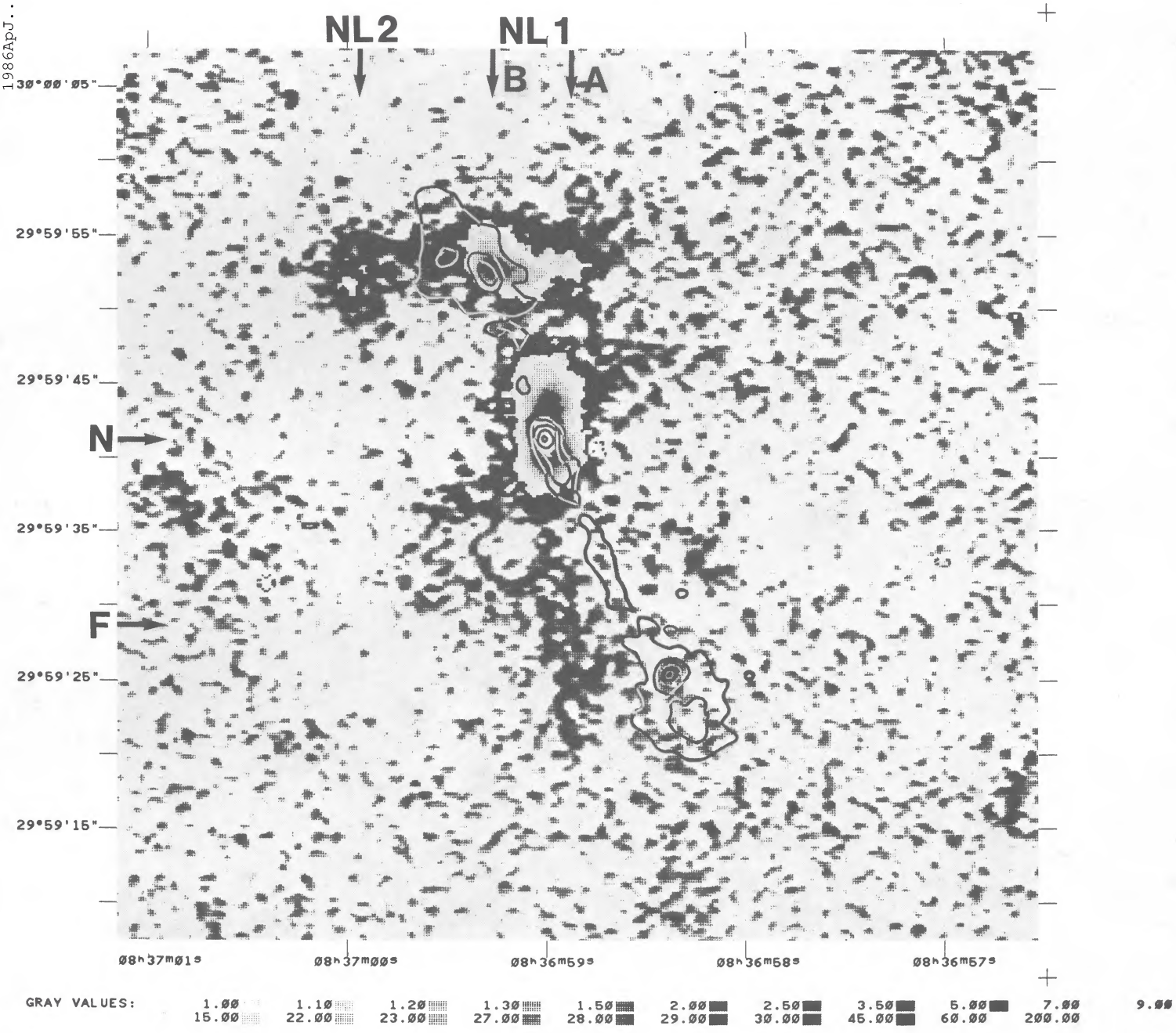

FIG. 7*a*

FIG. 7.—Gray-scale reproductions of the {Hα + [N II]} narrow-band image, with the galaxy continuum subtracted. The 6.2 cm radio map (0″.3 × 0″.3 resolution) is overlaid in (*a*), while (*b*) shows the 20.6 cm radio map (4″.5 × 4″.5 resolution). Contour values (mJy beam^{-1}) are (0.52, 2.1, 5.2, and 9.3), and (1.0, 1.9, 7.7, and 34.6), respectively. Individual emission-line regions are identified: NL1 and NL2 near the northern radio lobe, the central region N (near the nucleus), and the southern filament F.

ii) *Gas Kinematics*

The kinematics of gas in the emission-line regions was determined from the HGVS data using the [O III] λ5007 line (Figs. 9*a*, *c*), except along the faint southern filament, where this could be better determined from the Lick CCD data using the Hα emission line (Fig. 10). The principal results may be summarized as follows.

1. Within 5″ (~6 kpc) north and south of the nucleus (P.A. = 4°; Fig. 9*a*), the velocity changes smoothly (~150 km s^{-1} peak-to-peak). The nucleus is roughly the kinematic center of symmetry, the gas being redshifted to the north and blueshifted to the south. At P.A. = 85° through the nucleus (no figure shown), and within 5″ east and west of it, the total velocity change is less than 100 km s^{-1}.

2. At about 6″ (~7 kpc) north of the nucleus (Fig. 9*a*), the gas exhibits an abrupt increase of ~180 km s^{-1} in velocity. This jump occurs near the southern boundary of the northern radio hotspot. A similar jump occurs just north of this hotspot.

3. Along the southern filament the velocity gradually declines by ~80 km s^{-1} with respect to the nucleus, but subsequently rises to roughly its original value. A relatively sudden decrease of ~550 km s^{-1} (Fig. 10) occurs in the vicinity of the

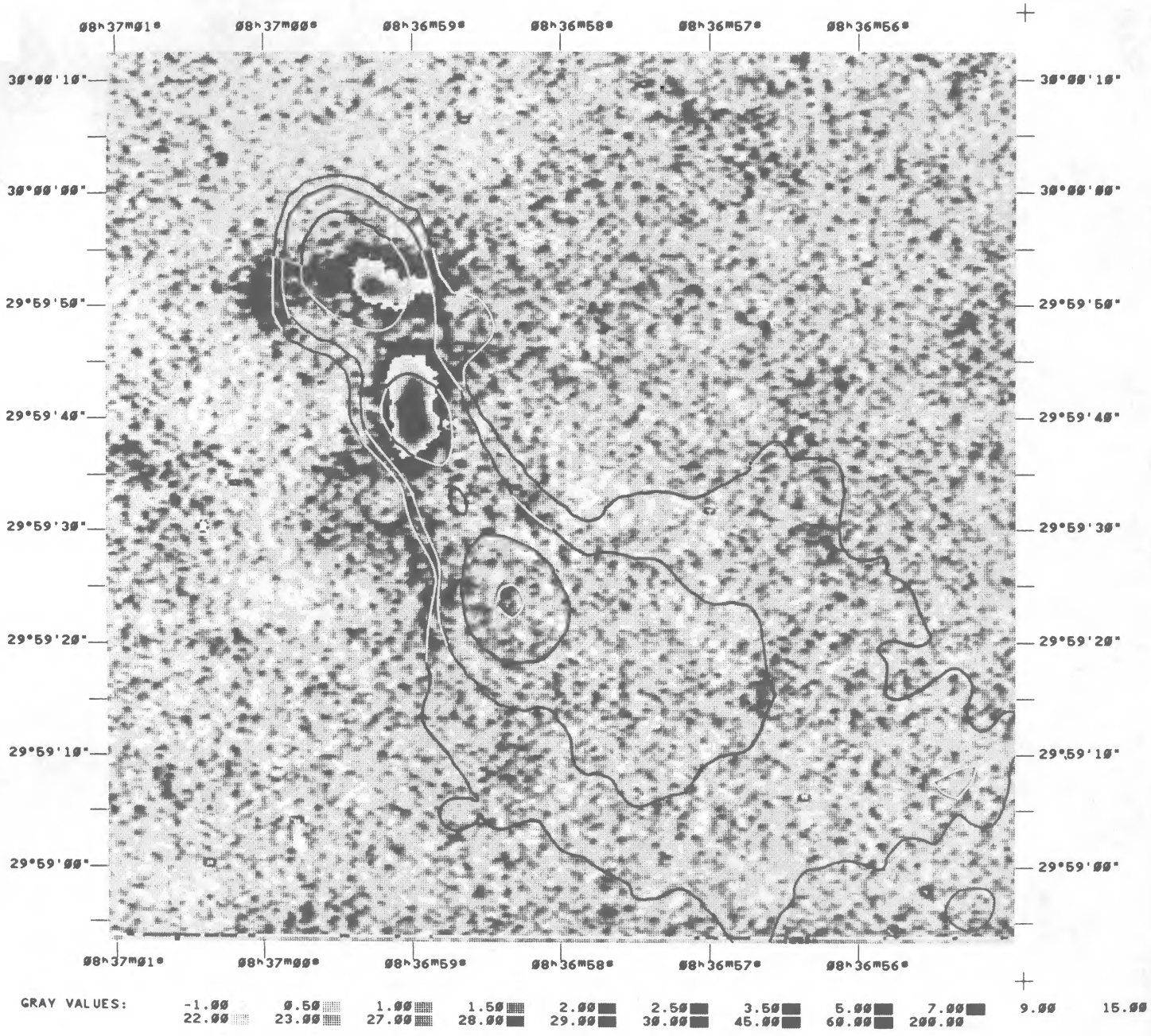

FIG. 7*b*

southern lobe (A), at ~15 kpc from the nucleus. The total range in velocities at P.A. = 4° is ~1100 km s^{-1}.

4. At P.A. = 95° through the northern radio lobe (Fig. 9*c*), another large jump in velocity is seen in the region close to the eastern boundary of the northern radio lobe, which is near the gap between the two emission-line regions NL1 and NL2. The gas at NL2 has an average radial velocity within ~30 km s^{-1} of that in the nucleus and exhibits a small velocity shift of ~70 km s^{-1} over its ~5″ length.

We conclude that ordered rotation is relatively unimportant in the gas kinematics. Instead, large velocity gradients exist near the boundaries of the radio source, and the emission-line regions (NL1, NL2, N, and F) appear to be kinematically distinct.

Plots of the emission-line widths (full width at half-maximum, FWHM) are shown in Figures 9*b* and 9*d*. They indicate that:

1. The line widths are ~250–400 km s^{-1} throughout most of the emission-line regions, in agreement with other radio sources having extended optical line emission.

2. The broadest lines (~600–750 km s^{-1}) are associated with the boundaries of the radio lobes, the same locations where the large velocity jumps are seen. These broad lines are not simply a consequence of atmospheric blurring of the emission lines seen on either side of the velocity jump; the velocities of the broad lines are not intermediate between the velocities on either side, and the lines are significantly wider than such a model would require (compare Figs. 9*a*, *b* and 9*c*, *d*).

Thus, neither the velocity field nor the line widths support simple models in which the emission-line gas consists primarily

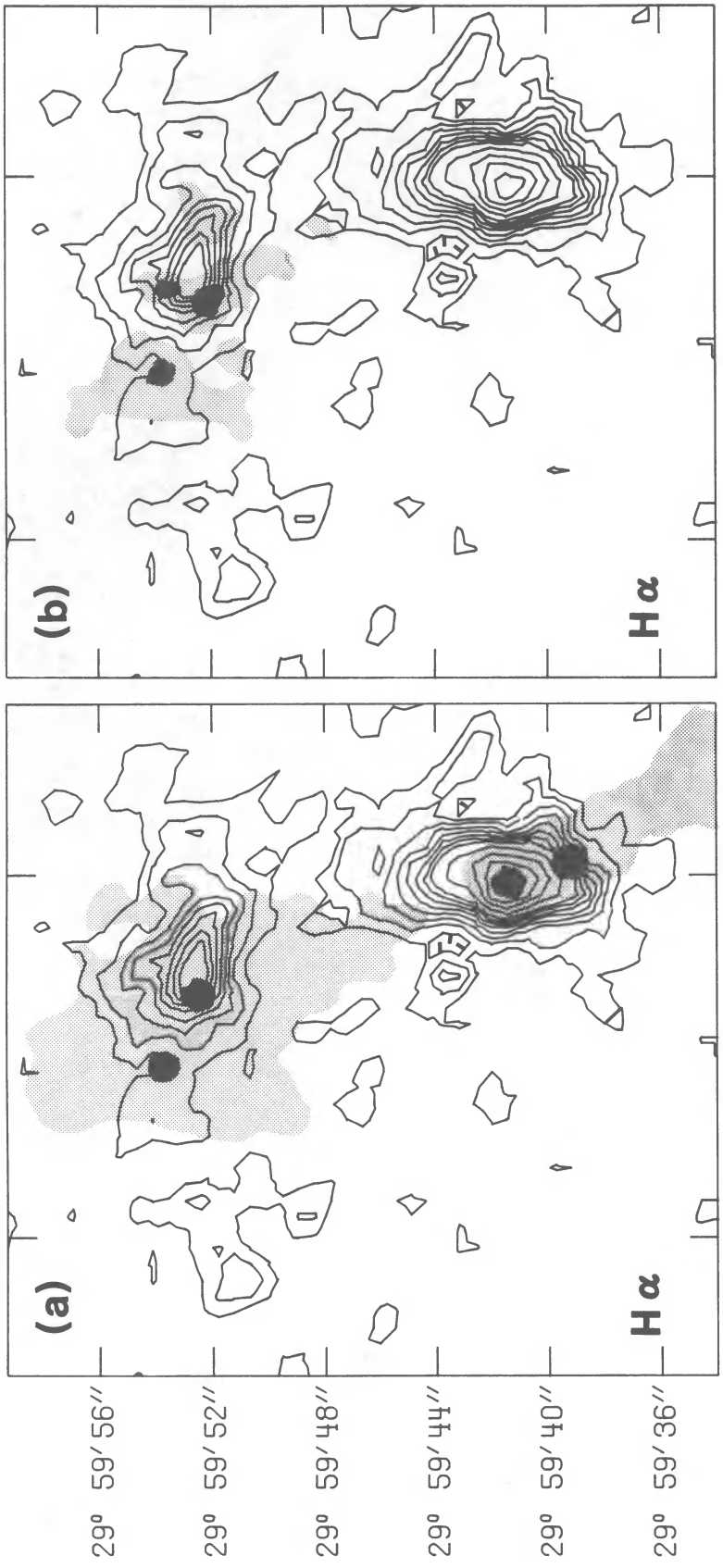

FIG. 8.—Gray-scale reproductions of the total and polarized intensities at 6.2 cm (1″.3 × 1″.3 resolution; [*a*, *c*] and [*b*, *d*], respectively), with video camera narrow-band images superposed (contours, {Hα + [N II]} in [*a*, *b*], and [O III] λ5007 in [*c*, *d*]). Contour values are linear, in arbitrary units; see Table 7 for absolute fluxes.

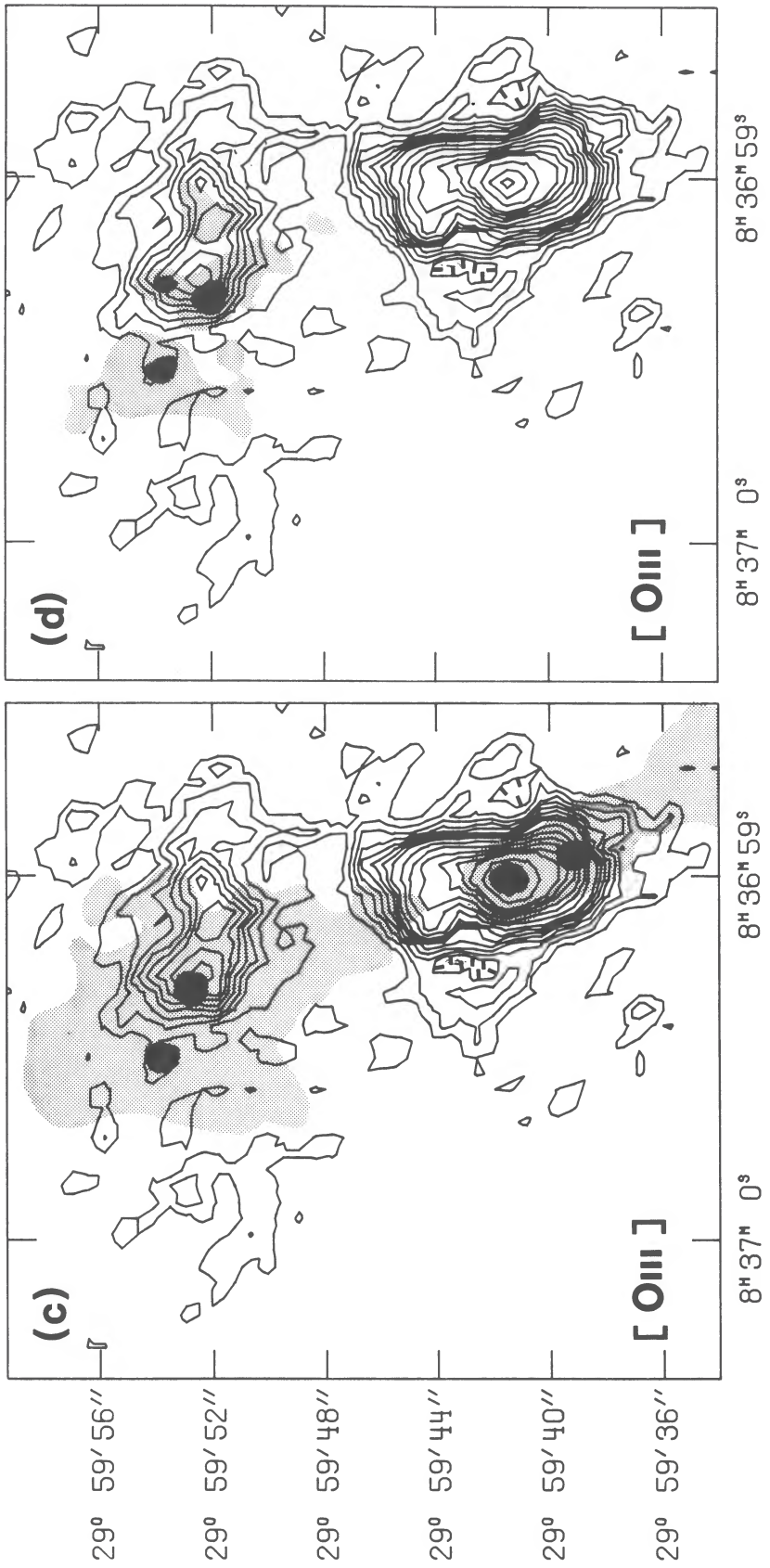

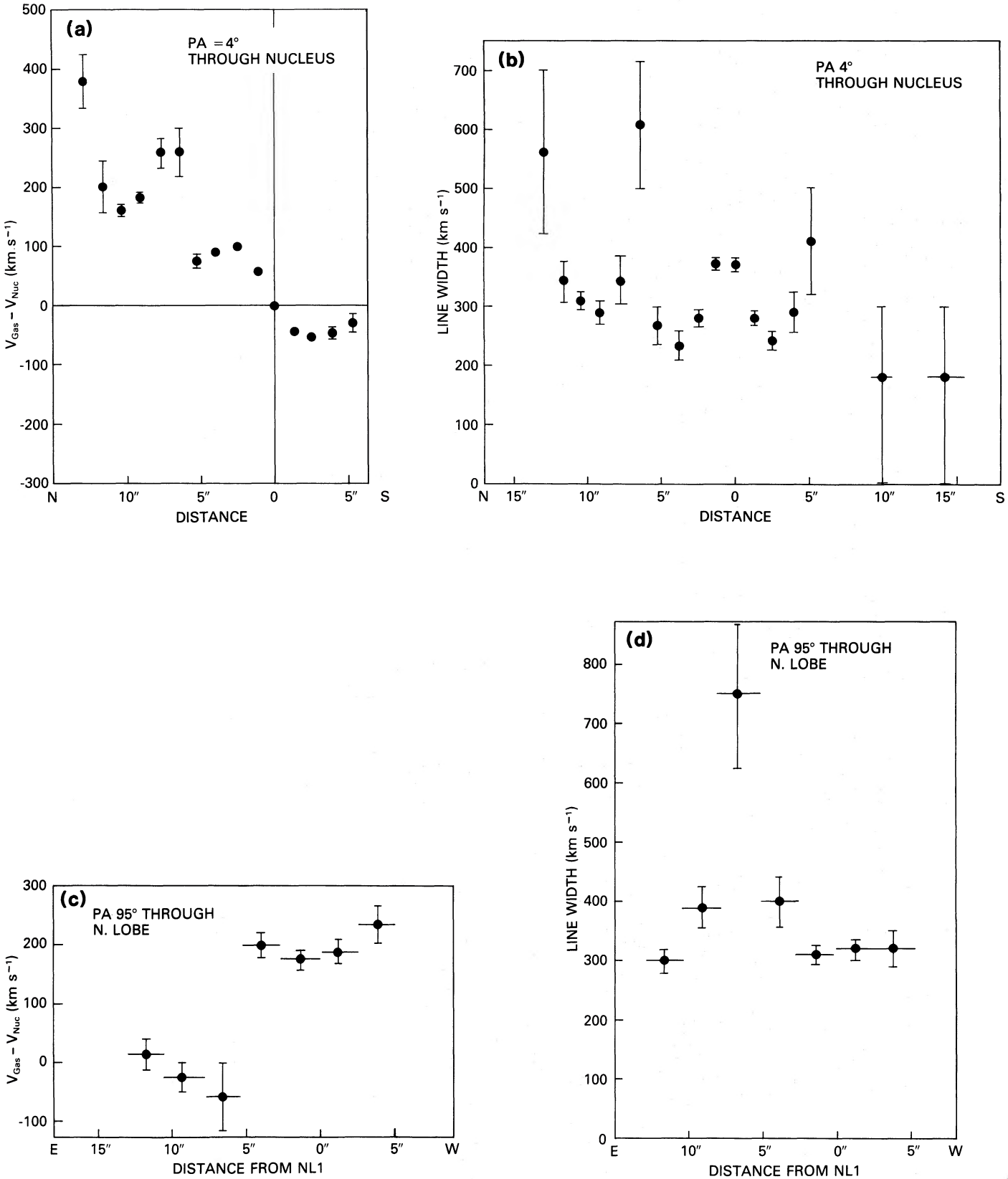

FIG. 9.—Velocities (cz) and velocity widths of the gas relative to the nucleus (cz = 19,300 km s^{-1}) along (*a*, *b*) P.A. = 4° through the nucleus, and (*c*, *d*) along P.A. = 95° through a position offset by 11″.0 to the north and 3″.2 to the east from the nucleus (i.e., through regions NL1 and NL2). The [O III] λ5007 line was measured in the HGVS spectra to derive these results. With the Lick CCD spectrograph, a large velocity gradient was found farther south along the filament (Fig. 10).

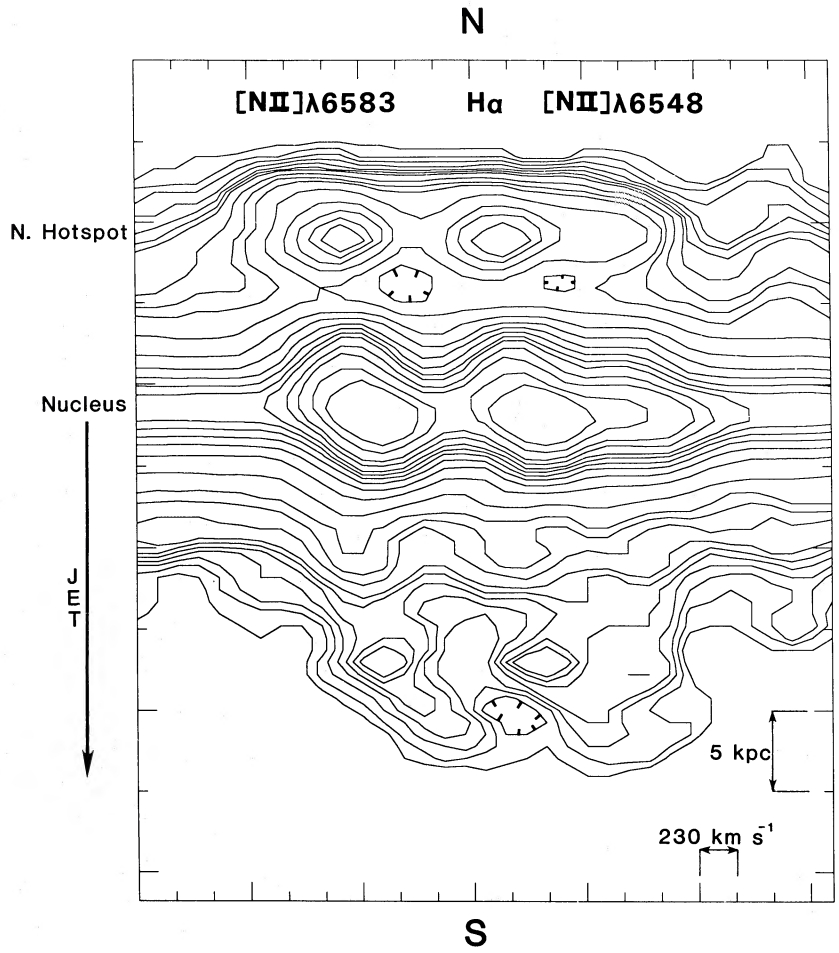

FIG. 10.—Contour representation of a one-dimensional slit spectrum taken with the Lick CCD spectrograph along P.A. = 4° through the nucleus and the faint southern filament. Contour values are arbitrarily chosen to show individual features. The spatial and dispersion directions are indicated, as are the three emission lines [N II] λ6583, Hα, and [N II] λ6548. The gas in the filament is blueshifted with respect to the nucleus. Note the large velocity gradient near the southern end ($\gtrsim$15 kpc from the nucleus).

of an ambient medium whose motion is unrelated to the radio source. Instead, the source seems to have a clear, though complex, effect on the gas kinematics.

iii) *Emission-Line Spectra*

Our data on the relative intensities of prominent emission lines in the nucleus (N) and the northern radio lobe (NL1) are summarized in Table 5. The flux-calibrated red Lick spectra are shown in Figures 11 and 12. Note the possible presence of an extremely faint, broad component of Hα emission similar to, but much weaker than, that in QSOs and type 1 Seyfert galaxies. Filippenko and Sargent (1985, 1986) detected such a feature in the nuclei of many bright, nearby galaxies. The spectral characteristics of the off-nuclear regions NL1A, NL1B, and NL2 are roughly comparable, except for their absolute intensities. An MMT spectrum of NL1 having lower resolution but covering a wider spectral range is illustrated in Figure 13. Only relative strengths of lines separated by *small* intervals can be deduced, since these data were not flux-calibrated.

The blue Lick ITS spectrum is shown in Figure 14*a*. A weak, featureless, nonstellar continuum (see § III*c*[iv] below) has been removed. Strong emission lines are present, but a rich absorption-line spectrum from the underlying starlight alters the apparent relative intensities of some lines and completely hides the weakest ones. Figure 14*b* shows the spectrum of an S0 template galaxy, IC 4889, on the same intensity scale but offset from that of 4C 29.30 for clarity. The data were obtained at Las Campanas Observatory near La Serena, Chile. The continuum shape and metallicity of IC 4889 were modified in the manner described by Filippenko and Halpern (1984) and Filippenko (1985), and weak [O II] λ3727 was excised from the spectrum. Reddening due to our Galaxy (Burstein and Heiles 1982) has been removed from both objects ($E_{B-V} = 0.02$ mag for 4C 29.30; $E_{B-V} = 0.03$ mag for IC 4889). The net emission-line spectrum of 4C 29.30, obtained by subtracting *b* from *a*, is illustrated in Figure 14*c*. It is clear that measurements of line intensities (Table 5) can now be made much more accurately. Note the presence of very weak Hγ, He II λ4686, and [Ne III] λ3967, which were previously not visible.

The flux-calibrated KPNO video camera images {(Hα + [N II] λλ6548, 6583); [O III] λ5007} and the red Lick long-slit spectra, when integrated over the same areas, are generally in good agreement ($\lesssim \pm 30\%$ difference). An exception is the nucleus, where the images give a much lower flux than the spectra. This may be due to the possible presence of a radial gradient in the stellar population, since we used the outer regions of 4C 29.30 to rescale the central portions of the images before subtracting the underlying starlight. The Lick data were

TABLE 5

RELATIVE INTENSITIES OF EMISSION LINES IN 4C 29.30

Line	Nucleus N[a]	N (no dust)[b]	Region NL1[c]	Seyfert 2[d]	LINER[e]
[Ne v] λ3426	<2[f]	<4[f]	...	10	...
[O II] λ3727	20	34	...	30	50
[Ne III] λ3869	7	11	...	15	2.8
Hγ λ4340	2	2.5	3	4.7	4.4
[O III] λ4363	<2[f]	<2.5[f]	≲1	2	≲0.6
He II λ4686	3	3	1.5	3	≲0.8
Hβ λ4861	10	10	10	10	10
[O III] λ5007	95	90	36	110	14
[N I] λ5200	2	2	1.5	1	1.4
He II λ5876	3	2	2	1	1.1
[O I] λ6300	8	5	7	5	8
Hα λ6563	51	28	33	29	28
[N II] λ6583	50	28	42	23	33
[S II] λ6716	17	9	18	7	10
[S II] λ6731	13	7	14	8	13

[a] Lick ITS 4″ × 4″ aperture. Stellar absorption lines removed (see text). Not dereddened.
[b] Nucleus dereddened, $E_{B-V} = 0.5$ mag.
[c] Stellar absorption lines not removed. Not dereddened.
[d] Koski 1978, Table 9. Dereddened.
[e] Ferland and Netzer 1983, Table 3. Dereddened.
[f] Line not detected: upper limit.

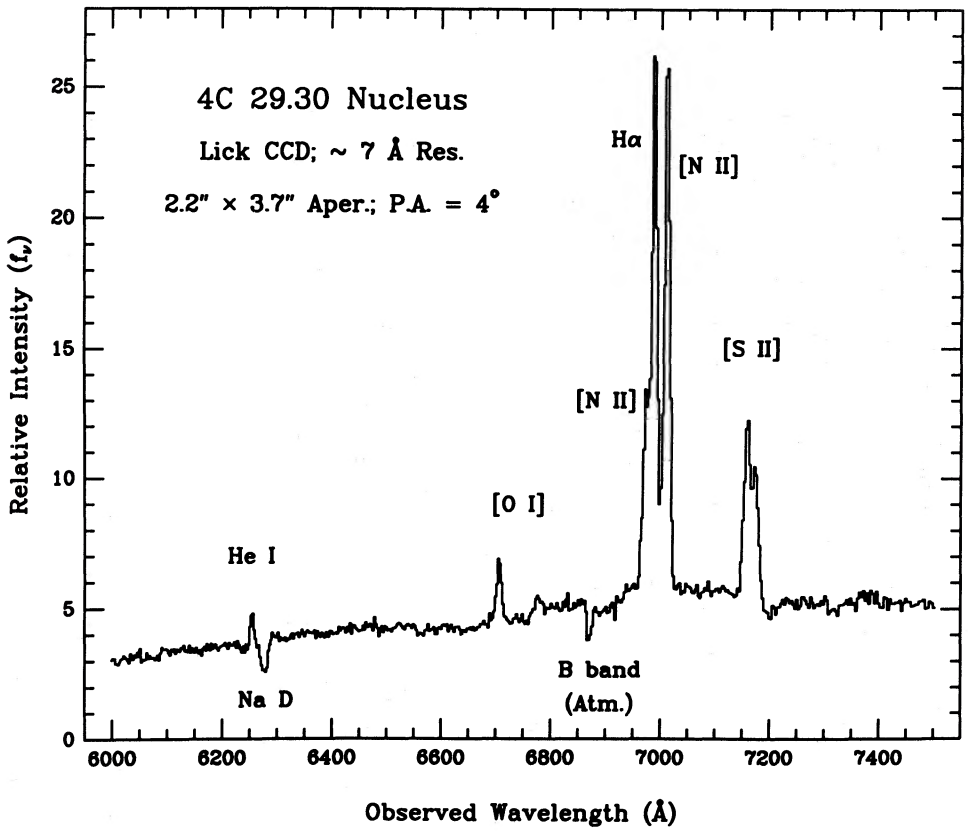

FIG. 11.—Red spectrum of the nucleus of 4C 29.30. Prominent emission lines, as well as Na I D absorption, are marked. A very faint, broad component of Hα emission may be present, but it must be confirmed with spectra in which atmospheric absorption lines (especially the B band) have been accurately removed.

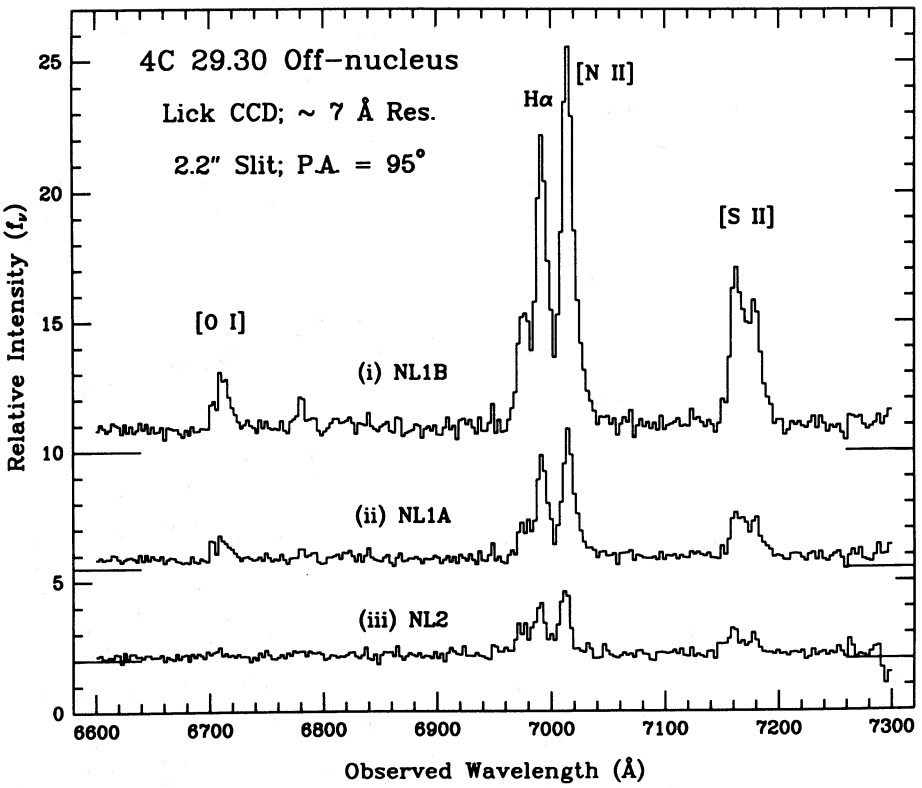

FIG. 12.—Red spectra of off-nuclear regions NL1B, NL1A, and NL2 in 4C 29.30 (see Fig. 7*a*). A slit of width 2″.2 was rotated to P.A. = 95°, and effective apertures having lengths of 8″.0, 6″.6, and 6″.6 (respectively) were used for the three regions. There may be a systematic offset of ~ +3 to 4 Å in the wavelength scale. The spectra are all plotted on the same intensity scale, with zero-points indicated by short horizontal segments. The relative strengths of [N II], [S II], [O I], and Hα are consistent with photoionization by nonstellar radiation, but their large absolute intensities (Tables 6, 7) suggest that this radiation does not originate in the nucleus.

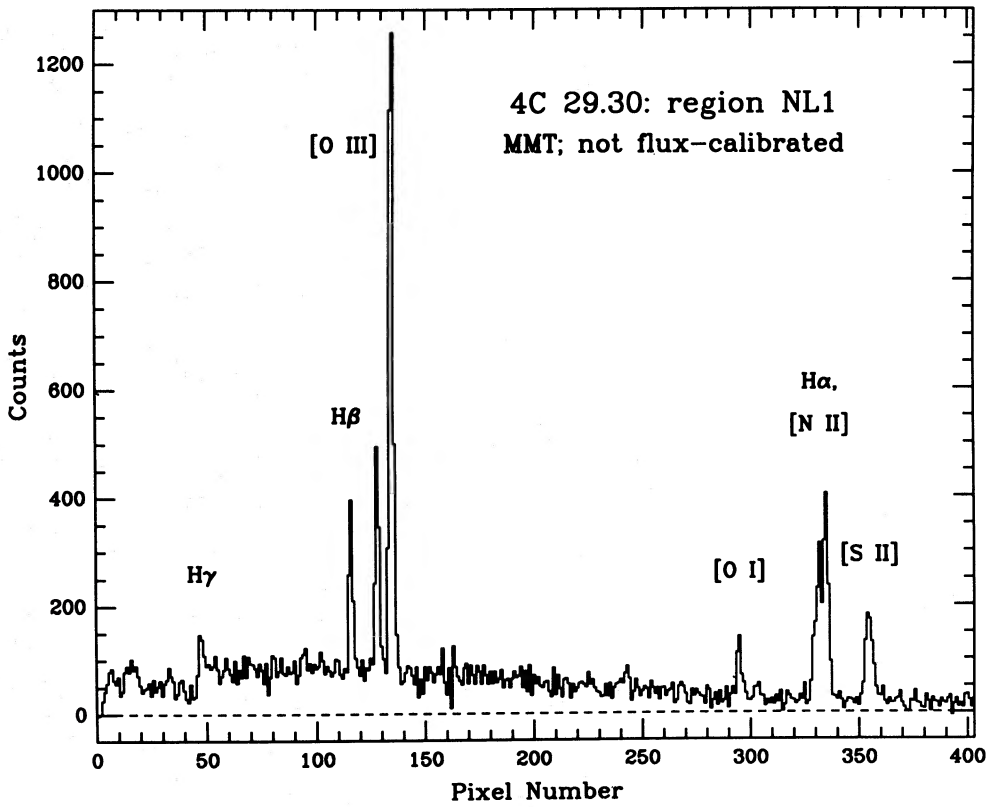

FIG. 13.—Uncalibrated MMT spectrum of the northern emission-line region NL1 in 4C 29.30. The integration time was 2 hr. Relative strengths of adjacent emission lines, but not those separated by many pixels, can be determined to first order. The observed ratios [O III]/Hβ, [N II]/Hα, and [O I]/Hα together imply that photoionization by a nonstellar continuum (rather than by UV radiation from hot stars) is the dominant excitation mechanism.

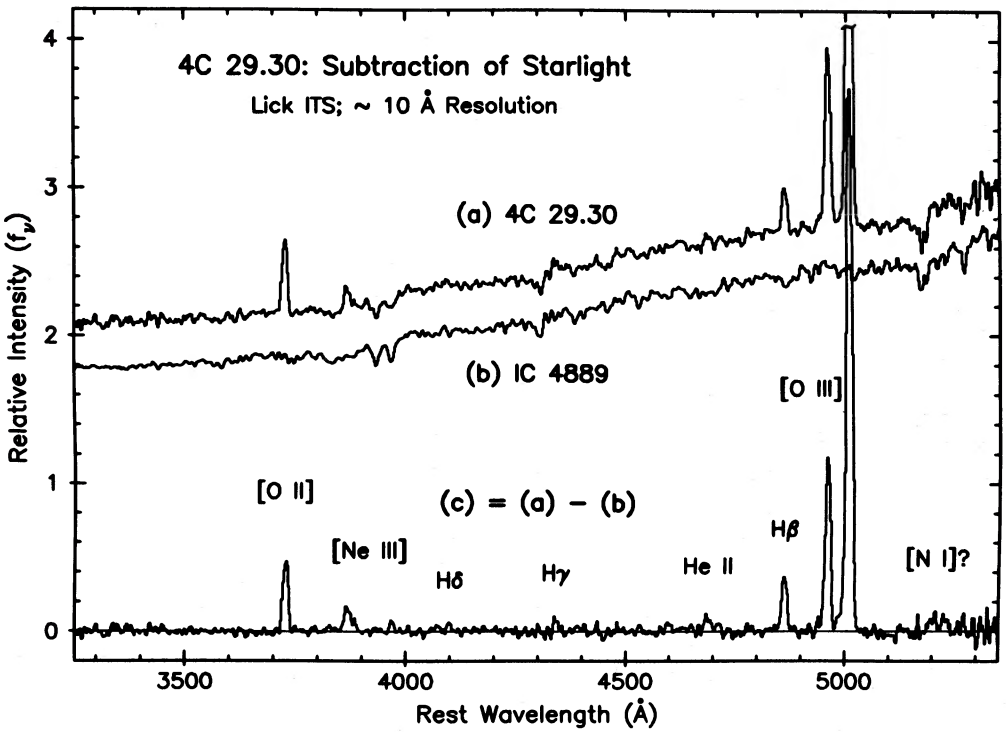

FIG. 14.—Dereddened spectra of (*a*) the nucleus of 4C 29.30, after removal of a nonstellar continuum similar to that in Fig. 15; (*b*) a template galaxy, IC 4889; and (*c*) the net emission-line component of 4C 29.30. All are shown on the same ordinate scale, but with different zero-point offsets. [O II] λ3727 has been artificially removed from the spectrum of IC 4889, and small adjustments have been made to the shape of the continuum and the metallicity to improve agreement with 4C 29.30. In (*c*), note the faint emission lines (e.g., He II λ4686, Hγ) which were previously hidden among absorption lines.

used to calibrate some of our other spectra on an absolute scale, and the results are listed in Table 6. The total (Hα + [N II]) and [O III] fluxes of the individual regions are given in Table 7A.

All these data lead to a number of key results.

1. The nuclear spectrum strongly resembles those of Seyfert 2 galaxies or narrow-line radio galaxies (e.g., Koski 1978; Cohen and Osterbrock 1981). The gas in the northern radio lobe is of significantly lower excitation ([O III] λ5007/Hβ ≈ 4), and appears intermediate in character between a Seyfert 2 and a LINER (Heckman 1980*b*; Ferland and Netzer 1983). The cryogenic camera and Lick CCD data indicate that the spectrum of NL2 is similar to that of NL1. Using standard emission-line diagnostics such as the line ratios [O I] λ6300/Hα, [N II] λ6583/Hα, and [O III] λ5007/Hβ (Baldwin, Phillips, and Terlevich 1981), we find that at all locations the spectrum is inconsistent with photoionization by ultraviolet radiation from hot stars.

2. The amount of reddening due to dust can be calculated from the observed Balmer decrement. Table 5 shows that Hα/Hβ ≈ 5.1 in the nucleus, whereas it should be ~3.1 (nearly the Case B value of ~2.9) if the gas is photoionized by a nonstellar continuum (Halpern and Steiner 1983; Ferland and Netzer 1983). 4C 29.30 has been detected as a strong ($\sim 6 \times 10^{10}\ L_\odot$)

TABLE 6

EMISSION-LINE FLUXES AND EQUIVALENT WIDTHS IN 4C 29.30[a]

	N. LOBE (NL1)		N.LOBE (NL2)		NUCLEUS (N)		FILAMENT (F)	
LINE (1)	$F/F\alpha$ (2)	E.W.	$F/F\alpha$ (3)	E.W.	$F/F\alpha$ (4)	E.W.	$F/F\alpha$ (5)	E.W.
[O I] λ6300	0.28	38	0.12	19	0.14	6	<0.1:	<7:
[N II] λ6548	0.45	58	0.38	63	0.39	15	~0.4	~30
Hα λ6563	1.00[b]	128	1.00[c]	167	1.00[d]	37	1.0[e]	69
[N II] λ6583	1.40	174	1.18	207	1.06	41	1.1	76
[S II] λ6716	0.62	82	0.43	69	0.35	15	~0.4:	~30:
[S II] λ6731	0.50	67	0.34	52	0.26	11	~0.3:	~20:

[a] See Fig. 7*a* for identifications of emission-line regions. E.W. given in Å units. Colon (:) denotes very uncertain measurement.

[b] $F\alpha \equiv F(\mathrm{H}\alpha) \approx 7.6 \times 10^{-15}$ ergs s^{-1} cm^{-2} through a 2.″2 × 15.″3 aperture.

[c] $F\alpha \equiv F(\mathrm{H}\alpha) \approx 1.4 \times 10^{-15}$ ergs s^{-1} cm^{-2} through a 2.″2 × 6.″6 aperture.

[d] $F\alpha \equiv F(\mathrm{H}\alpha) \approx 14 \times 10^{-15}$ ergs s^{-1} cm^{-2} through a 2.″2 × 3.″7 aperture.

[e] $F\alpha \equiv F(\mathrm{H}\alpha) \approx 0.59 \times 10^{-15}$ ergs s^{-1} cm^{-2} through a 2.″2 × 6.″6 aperture along filament in the vicinity of southern lobe A. Very low S/N ratio; all derived quantities for filament F (Table 7) are only rough estimates.

TABLE 7A

OBSERVATIONAL PARAMETERS OF EMISSION LINES

Component (1)	Area (2)	$F(\text{H}\alpha + [\text{N II}])$ (10^{-15} ergs s^{-1} cm^{-2}) (3)	$F([\text{O III}]\ \lambda5007)$ (10^{-15} ergs s^{-1} cm^{-2}) (4)	[S II] Ratio $F(\lambda6716)/F(\lambda6731)$ (5)
NL1	6″ × 9″	29	17	1.24 ± 0.20
NL2	6 × 6	7	2	1.26 ± 0.25
N	7 × 7	110	104	1.35 ± 0.15
F	2.2 × 15	3	...	1.3 ± 0.5
TS	20 × 40	210	170	1.3 ± 0.1

NOTES.—Cols. (1), (2): See Fig. 7*a* for identifications of emission-line regions. TS = total source; cols. (3), (4): Derived from the KPNO video camera observations (NL1 and NL2), the Lick CCD long-slit spectra (F), and a combination of these (N and TS); col. (5): Determined from the Lick CCD spectra.

TABLE 7B

PHYSICAL PARAMETERS OF THE OPTICAL EMISSION LINES

Component (1)	Hα Luminosity, $L(\text{H}\alpha)$ (10^{41} ergs s^{-1}) (2)	Estimated Volume, V (kpc^3) (3)	Electron Density, n_e (cm^{-3}) (4)	Filling Factor, f_f (10^{-6}) (5)	Mass Ionized Hydrogen, M ($10^6\ M_\odot$) (6)	Average Velocity, v_g (km s^{-1}) (7)	Kinetic Energy, K.E. (10^{53} ergs) (8)	Thermal Pressure, $P_g k^{-1}$ (10^6 K cm^{-3}) (9)
NL1	0.8	450	240	0.4	1.1	200	4	7
NL2	0.2	300	230	0.2	0.3	30	0.03	7
N	3.5	460	90	12	12	50	3	3
F	0.1	100	150	0.6	0.2	90–470	3	4

NOTES.—Col. (2): Hα luminosity estimated from col. (3) in Table 7A and the relative strengths in Table 6. Hα luminosity of entire source is $\sim 6.6 \times 10^{41}$ ergs s^{-1}, and total luminosity in all the emission lines is a factor of ~ 20 larger (Case B recombination). No values corrected for extinction or for underlying absorption lines (see text, § IIIc); col. (3): Volume assumed to be given by (area × shortest axis); see Table 7A; col. (4): Derived from the [S II] doublet ratio (Table 7A) and the calculations of Cantó *et al.* 1980 ($T_e = 15{,}000$ K); col. (5): Assume Case B recombination, $T_e = 15{,}000$ K, and gas density $n \approx n_e$; $f_f \approx 3.9 \times 10^{24} L(\text{H}\alpha) V^{-1} n_e^{-2}$; col. (6): $M = m_p n_e V f_f \approx 3.2 \times 10^{-33} L(\text{H}\alpha) n_e^{-1}\ M_\odot$, where m_p is the mass of the proton; col. (7): Average bulk velocities of gas are estimated from Figs. 9 and 10; col. (8): K.E. $= 0.5\ M v_g^2$. In filament F, most of the kinetic energy is in the component having the highest velocity; col. (9): $P_g k^{-1} = 2 n_e T_e$.

far-infrared source by *IRAS* (Lonsdale *et al.* 1985), which also indicates the presence of dust. Our observed ratio of Hα/Hβ suggests that $E_{B-V} \approx 0.5$ mag. The very low Hγ/Hβ ratio, on the other hand, implies that $E_{B-V} \approx 1.6$ mag. This discrepancy can be understood if the stellar continuum in the nucleus is characterized by Balmer absorption lines which are stronger than in normal elliptical galaxies or in the bulges of early-type spirals. The Allen (1979) method could be used to obtain an estimate of the reddening, but we do not have accurate measurements of the [O II] λλ7319, 7330 or the [S II] λλ4069, 4076 lines. Since the Hβ emission line is affected more by absorption than the Hα line, and Hγ much more than Hβ, it is likely that the reddening in the nucleus of 4C 29.30 is roughly $E_{B-V} \approx$ 0.4–0.5 mag, but a conservative upper limit is $E_{B-V} \approx 1.1$ mag. Note that the spectrum of the nucleus (Table 5) bears a striking resemblance to that of a typical Seyfert 2 galaxy when it is dereddened by $E_{B-V} \approx 0.5$ mag, whereas a color excess of ~ 0.0 mag or ~ 1.1 mag gives much worse agreement.

The reddening in the northern lobe appears to be considerably less than that in the nucleus, since Hα/Hβ/Hγ ≈ 3.6/1.0/0.3 instead of the expected recombination decrement 3.1/1.0/0.46. Once again, Balmer absorption lines probably affect the emission-line intensities. In the discussions to follow, we will not attempt to correct the data for reddening, except in situations where the reddening could seriously alter the conclusions.

3. Upper limits to the [O III] λ4363 emission line in spectra of the nucleus and NL1 (Table 5) yield upper limits to the electron temperature (T_e) in these regions of $\sim 15{,}000$ K and $\sim 17{,}000$ K, respectively, if $n_e \lesssim 10^4$ cm^{-3} (see Fig. 11 of Filippenko and Halpern 1984). Collisional heating by shocks can probably be eliminated as the dominant excitation mechanism for the emission-line gas in both cases, since shock models generally give $T_e \gtrsim 30{,}000$–$40{,}000$ K in the [O III] zone (e.g., Shull and McKee 1979). Although dereddening the emission lines increases the observed ratio [O III] λ5007/[O III] λ4363, we find that $T_e \lesssim 21{,}000$ K in the nucleus and $T_e \lesssim 26{,}000$ K in NL1 even if $E_{B-V} \approx 1.1$ mag; thus, our conclusions regarding the excitation mechanism remain unchanged, especially if we adopt the more reasonable value $E_{B-V} \approx 0.5$ mag.

iv) *Continuum*

Several methods were employed to estimate the fractional contribution of a featureless blue component to the continuum in the nucleus. First, the equivalent widths of the three strongest absorption lines in the nucleus (the G band at $\sim$λ4304, Mg I *b* λ5175, and Na I D λ5892) were determined. The average equivalent width (E.W.) of these lines is 5 ± 1 Å, compared with an expected average of ~ 6.5 Å in luminous early-type galaxies (Heckman 1980*a*). This suggests that the featureless component contributes $\sim 23\% \pm 15\%$ of the total flux at λ5400, but the true uncertainty may be even larger since substantial differences in equivalent widths of absorption lines are seen even in normal galaxies.

Second, the continuum from the nucleus of 4C 29.30 (Lick ITS data) was decomposed into a nonstellar power law ($f_\nu \propto \nu^{-\alpha}$) and the spectrum of an "average" giant elliptical galaxy (Yee and Oke 1978), as described in detail by Halpern and Filippenko (1984). Ignoring regions contaminated by emission lines, least-squares fits were performed to obtain the reddening and the ratio of nonstellar to total flux at λ5400, for various values of α. An accurate determination of the spectral index

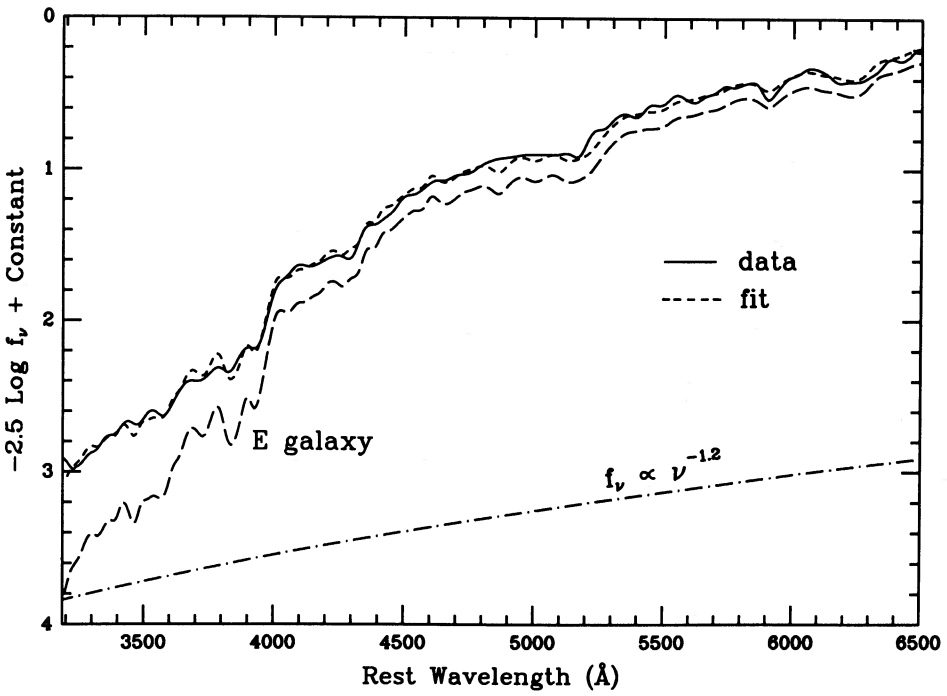

FIG. 15.—The heavily smoothed, dereddened ($E_{B-V} = 0.1$ mag) continuum from the nucleus of 4C 29.30 (*solid line*) is decomposed into a nonstellar power law of index 1.2 (*dot-dashed line*) and the spectrum of an average giant elliptical galaxy (*dashed line*). A dotted line represents the best least-squares fit to the data, which were obtained with the Lick ITS through a 4″ × 4″ aperture. Each numbered tick mark of the ordinate scale corresponds to one magnitude.

was impossible due to the dominance of starlight, the probable presence of hot young stars, and the small wavelength range, but $\alpha = 1.2 \pm 1.0$ produced good results. This is fairly representative of Seyfert galaxies (Koski 1978; Malkan and Filippenko 1983). As illustrated in Figure 15, at visual wavelengths the nonstellar continuum is very weak; it contributes only ~10% of the total flux at λ5400, in rough agreement with the results derived from the measured equivalent widths of stellar absorption lines. At λ3200, however, its strength is comparable to that of starlight. The amount of ionizing luminosity provided by this power law is $\sim 6.6 \times 10^{42}$ ergs s^{-1}, uncorrected for extinction. Although a reddening of $E_{B-V} \approx 0.1$ mag ($A_V \approx 0.3$ mag) for the total continuum of 4C 29.30 was formally derived during the fitting procedure, this result is very uncertain. In fact, it is quite likely that the stellar and nonstellar continua are actually reddened by somewhat different amounts.

Finally, the strength of the nuclear nonstellar continuum at a rest wavelength of 5400 Å can be estimated from the observed strengths of the Hα emission line and the total (stellar plus nonstellar) continuum at λ5400. Using the Lick ITS spectrum of the central 4″ × 4″, we find that $f_\nu(\lambda 5400) \approx 4.3 \times 10^{-27}$ ergs s^{-1} cm^{-2} Hz^{-1}. If *all* of this radiation were nonstellar, and if $f_\nu \propto \nu^{-1.2}$ even at energies near and beyond the Lyman limit, then the intensity of Hα should be $I(\mathrm{H}\alpha) \approx 6.7 \times 10^{-14} f_c$ ergs s^{-1} cm^{-2}, where f_c is the covering factor of the clouds of gas that produce the emission lines. The measured flux in the ITS spectrum is $I(\mathrm{H}\alpha) \approx 1.3 \times 10^{-14}$ ergs s^{-1} cm^{-2}, or ~20% of the predicted value when $f_c = 1$. Hence, at least ~20% of the observed continuum at λ5400 must be nonstellar, unless $\alpha < 1.2$ near the Lyman limit. This value is quite comparable to that obtained with the other two methods. Of course, if $f_c \lesssim 0.2$, then a much stronger ionizing continuum (perhaps in the form of a "UV bump"; Malkan and Sargent 1982) is needed to account for the Hα flux, as is the case in several other low-luminosity active galactic nuclei (see, e.g., Filippenko 1985).

The optical continuum far from the nucleus appears to be significantly bluer than that of the nuclear region. Our [O III] λ5007 and Hα off-band video camera frames, with central bandpass wavelengths of 5422 Å and 6826 Å, respectively, indicate that between these wavelengths the continuum within 2″ of the nucleus is ~17% redder than the continuum in the annulus extending 2″ to 8″ from the nucleus. This agrees with the cryogenic camera spectra, in which the continuum 11″ north of the nucleus (in an 11.″2 × 2.″5 aperture) is ~19% bluer than the nuclear continuum (in an 8″ × 2.″5 aperture) between 5400 Å and 6800 Å.

The Na I D λ5892 (E.W. = 5 ± 2 Å) and possibly Mg I *b* λ5175 absorption lines are seen in our cryogenic camera spectrum of the 11.″2 × 2.″5 region 11″ north of the nucleus. Although the D line can be produced by interstellar gas, part of it can probably be attributed to starlight. Moreover, the Mg *b* triplet is not related to the interstellar medium; hence, much of the off-nuclear continuum is presumably starlight. Its relatively blue color suggests the presence of a hot (young) stellar component.

We also note that the off-band video camera frames show no excess optical continuum associated with any of the radio knots. In particular, we can set an upper limit of ~8.5 μJy at 6826 Å and ~4.8 μJy at 5400 Å for any nonthermal optical continuum associated with the radio knots D1 and D2.

v) *Physical Parameters of the Gas*

Assuming a Case B recombination spectrum, $T_e \approx 15{,}000$ K, and precepts similar to those described in our previous papers, we have derived various physical parameters of the emission-line gas (Table 7B). Our MMT and Lick spectra of the [S II]

$\lambda\lambda$6716, 6731 lines show that the gas is near the low-density limit (Table 7A), yielding estimates (Cantó *et al.* 1980) of the electron density n_e.

The thermal pressures of the emission-line gas ($P_g k^{-1} = 2n_e T_e$) in the various regions [Table 7B, col. (9)], as well as the pressures in the adjacent radio-emitting plasma [Table 4B, col. (5)], are very uncertain, but they are consistent with the conclusion that the two media may be in pressure equilibrium. Perhaps the pressure in the most compact radio components (C1, C2, D1, D2) is higher than that of the surrounding gas. We have found similar results in 3C 305 and 3C 277.3.

IV. DISCUSSION

a) Optical/Radio Relationships

Our observations show that the optical line-emitting gas and the radio continuum in 4C 29.30 are clearly related, and they strongly suggest the interaction of the source with a relatively dense gaseous environment. The evidence for this can be summarized as follows.

1. The optical emission-line gas is found adjacent to bright radio knots and/or along the boundaries of the source (Figs. 7 and 8). This is precisely where the jets and lobes could be expected to interact with their environment (e.g., Begelman, Blandford, and Rees 1984).

2. Northeast of the bright emission-line region NL1, the source appears bent and decollimated (Figs. 1 and 8), rather similar to the southern jet in 3C 277.3 (van Breugel *et al.* 1985*a*). This might be expected in a collision between a northern jet and dense ambient gas.

3. The absence of radio source polarization is roughly correlated with the presence of emission-line gas (Figs. 5 and 8). One explanation is that the ionized gas may be partially entrained in the boundaries of the source, causing an inhomogeneous "Faraday screen" to depolarize the underlying radio emission.

4. Peculiar gas kinematics are visible, with strong velocity gradients, velocities well in excess of the escape velocity at some locations, and very broad lines preferentially near the boundaries of the source (Figs. 9 and 10). A possible cause is the entrainment of ambient gas by the jet and lobes in their boundary layers.

5. The emission-line gas far from the nucleus cannot be photoionized by continuum radiation from the nucleus (see § IV*c* below); rather, it requires a locally generated heating source. It seems natural to suppose that this source of ionization is related to the jet/gas interactions.

6. The total emission-line luminosity of the northern regions NL1 + NL2 ($\sim 2 \times 10^{42}$ ergs s^{-1}; Table 7) exceeds that of the radio luminosity ($\sim 2.1 \times 10^{41}$ ergs s^{-1}; Table 4) by a factor of ~ 10. The analogous ratio for the entire source is even larger. Thus, the radio emission constitutes only a small fraction ($\lesssim 10\%$) of the total energy that is dissipated in the jet/gas interactions. Most of the energy is probably used to heat and accelerate the ambient gas.

7. The observations suggest that the ionized gas and the (diffuse?) radio-emitting plasma may be in pressure equilibrium. If true, this would be consistent with the presence of entrained ambient gas in the boundary layers (cocoons) of the jets.

8. The optical morphology of the galaxy is highly disturbed (Fig. 6), perhaps because of the recent capture of a gas-rich disk galaxy (see § IV*b* below). This captured gas could then be illuminated and excited by the radio source.

These radio and optical properties are very similar to those of other radio galaxies associated with extended emission-line regions. They confirm and strengthen our previous conclusions on the general characteristics of such objects. On the other hand, 4C 29.30 also has unique properties which may highlight some of the processes involved in the interaction of a radio galaxy with its environment, as we will now discuss.

b) Origin of the Gas

General, but mostly indirect, arguments indicate that the emission-line gas associated with radio galaxies is of a local (interstellar) origin, rather than ejected from the parent galactic nuclei; the gas is not a generic component of the jet fluid (van Breugel *et al.* 1985*a*; van Breugel 1986). The exact nature of such gas, however, is often unclear. Our optical images of 4C 29.30 strongly suggest that in this object the gas may be debris from a gas-rich galaxy which merged with the primary galaxy. Various "loops" or partial "shells" are visible around the object (Fig. 6*b*), and a relatively blue secondary nucleus seems to be present. Moreover, the nuclear region exhibits a dust lane (Fig. 6*c*), and the faint, ringlike extensions of the [O III] λ5007 emission (Figs. 8*c* and 8*d*) may be evidence of a disk or ring of ionized gas encircling the nucleus.

Optical shells have recently been found around several nearby elliptical galaxies (Malin and Carter 1983). Quinn (1984) has shown that these may be caused by the capture of a disk galaxy (but see Williams and Christiansen 1985 for a different explanation). More detailed models by Hernquist and Quinn (1986*a*, *b*) show that clean, distinct shells occur only under somewhat special circumstances, but that loops, tails, arcs, fans, plumes, and other peculiar features would be more common. This is partly due to the importance of projection effects, and partly to the use of more realistic models. Other studies (e.g., Toomre and Toomre 1972; Merritt and de Zeeuw 1983) help confirm these conclusions. A merger interpretation for 4C 29.30 is supported by the presence of the central disk or ring near its nucleus, as well as by its blue secondary nucleus, both of which could be the remnants of the captured disk galaxy. In fact, the captured gas might even have triggered the nuclear activity which produced the radio source.

c) Excitation and Energetics of the Gas

The gas near the nucleus can plausibly be interpreted as material that is photoionized by the ultraviolet continuation of the nonstellar optical radiation detected in the nucleus (Fig. 15); the emission-line spectrum strongly resembles the spectra of type 2 Seyfert nuclei (Table 5), which are well represented by such photoionization models. Furthermore, the inferred ionizing luminosity of the nonstellar continuum ($\sim 6.6 \times 10^{42}$ ergs s^{-1}; § III*c*[iii]) is comparable to the nuclear emission line luminosity ($\sim 7.0 \times 10^{42}$ ergs s^{-1}; Table 7B).

This simple model, however, is probably inadequate to explain the bright regions associated with the northern radio lobe. As seen from the nucleus, the bright region NL1 could cover no more than $\sim 3\%$ of the sky, while the fainter region NL2 could cover $\lesssim 1\%$. Since the emission-line luminosities of NL1 and NL2 are $\sim 1.6 \times 10^{42}$ ergs s^{-1} and $\sim 4.0 \times 10^{41}$ ergs s^{-1}, respectively, the ionizing luminosity from the nucleus would have to exceed $\sim 5 \times 10^{43}$ ergs s^{-1} to photoionize these regions, unless the radiation were somehow preferentially beamed toward NL1 and NL2. This is larger than the inferred ionizing luminosity by a factor of ~ 8, even if clouds of gas near the *nucleus* do not absorb *any* of the nonstellar continuum as it

travels toward NL1 and NL2. The gas in NL1 and NL2 is therefore unlikely to be photoionized by nonstellar radiation emitted by the nucleus. Instead, the close morphological connection between the radio source and the emission-line gas implies that the gas is somehow excited by the radio source itself.

A nonthermal ionizing continuum associated with the radio knots D1 and D2 would need a spectral index of $\lesssim 0.6$ between the radio and ultraviolet frequencies to provide adequate ionizing radiation for NL1. This is a significantly flatter spectrum than is observed at longer wavelengths ($\alpha_6^{21} \approx 0.9$; Table 4). More importantly, the flux density of such a nonthermal continuum at 5400 Å would be $\gtrsim 15$ μJy, in violation of the observed limits ($\lesssim 4.8$ μJy) on any excess optical continuum associated with D1 and D2. We conclude that the ionization of gas in the northern regions NL1 and NL2 is *not* caused by ultraviolet synchrotron radiation.

Collisional ionization of the gas in NL1 by shock heating also seems to be ruled out, since the upper limit on the temperature of the O^{++} zone ($T_e \lesssim 17{,}000$ K or $\lesssim 26{,}000$ K if $E_{B-V} \approx 1.1$ mag) falls below the predicted temperature ($\gtrsim 30{,}000$ K). A more accurate measurement of I([O III] λ4363) in spectra of higher quality must be made to confirm this conclusion.

Ferland and Mushotzky (1984) have recently calculated models in which gas is heated and ionized by relativistic particles. They have applied them to several cases of optical emission-line filaments embedded in synchrotron nebulae (e.g., Cen A and the Crab Nebula), and find that heating by relativistic particles can have a significant impact on the emission-line spectrum. A complication with such models for 4C 29.30 is that emission-line gas also exists well away from the radio source, especially in the northern region NL1 and the southern filament F (Fig. 7*a*).

One plausible alternative for the ionization in the northern regions of 4C 29.30 is photoionization by thermal (X-ray) radiation from hot ($\gtrsim 10^6$ K). gas. This gas could have been heated to high temperatures by the bow shock driven by the radio source as it plowed through the ambient interstellar medium (Norman *et al.* 1982; van Breugel *et al.* 1985*a*). The emission-line gas itself could represent the relatively dense component of the ambient medium (the "clouds," *c*) which was only heated to modest temperatures, while the diffuse intercloud (*ic*) medium would have had shocks of much higher velocity [$v_{ic} = v_c(n_c/n_{ic})^{1/2}$] driven into it, thereby producing much higher temperatures (McCray and Snow 1979; McKee and Hollenbach 1980). If this shocked intercloud gas emits enough radiation to photoionize the emission-line gas, then $L_X \gtrsim 10^{43}$ ergs s^{-1}, which should be detectable with X-ray satellites since $f_X \gtrsim 10^{-12}$ ergs s^{-1} cm^{-2}.

It is obvious from the above discussion that the source of ionization for the extended, extranuclear emission-line regions is not well understood. No matter how the radio source ionizes the gas, however, far more of the energy carried by the jets in 4C 29.30 is ultimately converted into line emission than into radio synchrotron emission; the ratio of total emission-line luminosity to total radio luminosity, L_{lines}/L_{radio}, is at least 10 both in the northern lobe and globally. Because it is highly unlikely that the conversion to emission lines occurs with perfect efficiency, we conclude that $\lesssim 10\%$ of the energy in the jets is dissipated in the form of radio synchrotron emission. This low value is similar to our result for 3C 305 (Heckman *et al.* 1982), and in agreement with various ad hoc theoretical estimates of the efficiencies of radio synchrotron production in radio galaxies [see O'Dea (1985) for a recent discussion].

In other radio sources with extended optical line emission, the ratio L_{lines}/L_{radio} ranges from ~ 1 in 3C 277.3, 3C 171, and NGC 7385 (van Breugel, Heckman, and Miley 1984; Heckman, van Breugel, and Miley 1984; Simkin, Bicknell, and Bosma 1984) to ~ 10 in 3C 305, 4C 26.42, and Minkowski's Object (Heckman *et al.* 1982; van Breugel, Miley, and Heckman 1984; van Breugel *et al.* 1985*b*). While there clearly exist radio sources with $L_{lines}/L_{radio} \ll 1$, we speculate that the jets in these sources are nevertheless inefficient at producing radio emission; in the absence of a dense, local gaseous medium, the missing energy must somehow be disposed of in a tenuous and very hot environment.

d) Radio and Optical Morphology

i) *Misalignment of the Optical Filament and the Radio Jet*

One of the most puzzling results from our observations is the $\sim 20°$ misalignment between the southern radio jet and the optical emission-line filament. There is only marginal evidence for radio emission between these regions, and the best proof that they are actually related comes from the large velocity gradient along the filament.[6] Could it be that there is a large, invisible component to the outflow from the nucleus of 4C 29.30?

Blandford and Payne (1982) have suggested that extragalactic radio sources might be produced by hydromagnetic flows from accretion disks. Most of the power is concentrated in the jet center, while most of the angular momentum and magnetic flux from the disk are carried in the outer regions of the jet and serve to confine it. The discovery of rotating molecular disks at the bases of some Galactic bipolar outflows has led to similar models for stellar jets (Pudritz and Norman 1986). In these models a jet of highly ionized gas is radiatively driven by the newly formed star, and the outer molecular flow is caused by a hydromagnetic wind from the molecular disk.

By analogy, the radio jet in 4C 29.30 might only be the high-energy part of a much larger outflow from the nucleus. The emission-line filament could be the outer edge of a cool, radio-quiet cocoon surrounding the jet. Its excitation and velocity gradient might be due to the entrainment of ambient gas by this cocoon. A definitive prediction of these models is that the material in the cocoon should rotate around the axis of the jet (Pudritz and Norman 1986), as in the bipolar molecular flow of L1551 (Uchida *et al.* 1986). This might be amenable to testing in 4C 29.30 by further optical observations.

A different origin for a cocoon between the radio jet and the emission-line filament may be backflow from the terminal shock (A2) of the jet. Detailed calculations of hydrodynamic models (Norman *et al.* 1982; see also Smarr, Norman, and Winkler 1984) have shown that cocoon-dominated jets occur in jets of low density and high Mach number. An important feature of such models is that shocks external to the jet are in the cocoon, rather than the ambient medium, and that the

[6] As in 4C 26.42, we suspect that the jet in 4C 29.30 is partially surrounded by a shell of ionized gas. This shell appears bright (like a "filament") at one edge because of the longer lines of sight through the ionized gas there. That no such filament is observed on the other side of the jet may be due to slightly asymmetrical external (ram) pressure of the ambient medium. This is indicated by the radio source structure, which exhibits its largest intensity gradients to the NE, suggesting motion of the galaxy in that direction. The resulting extra ram pressure on this side will rub the ambient gas against the jet or its surrounding cocoon.

backflowing material is accompanied by efficient entrainment of the denser surrounding gas into the cocoon. When applied to the southern jet in 4C 29.30, however, it is not clear why the emission-line filament is farthest from the jet axis near A2 (the presumed Mach disk in such a model) and converges toward the jet near the nucleus, and why there is no radio emission associated with these shocks within the cocoon. In fact, we will now suggest a different explanation for the radio knots in the southern jet.

ii) *Evidence for Shocks*

The knots in the southern jet and in its partially visible counterpart to the north (Figs. 1, 2, and 3) suggest that shocks occur in the jets, since (*a*) the bright knots A2 and D1 are elongated perpendicular to the jet directions; (*b*) the magnetic fields at these locations are transverse to the jet orientations; and (*c*) "upstream" the knots have large intensity gradients (A2, C2, D1) while "downstream" the jets widen or decollimate (A1, C1, D2, and D3). These properties resemble those of the M87 jet (Owen, Hardee, and Bignell 1980; Biretta, Owen, and Hardee 1983).

On a relatively large scale (1".3; Fig. 1) it appears as though the knots in 4C 29.30 come in pairs. At higher resolution (0".3; Figs. 2 and 3) the inner knot in lobe D again breaks up into a close pair (D1, D2). Other sources with bright pairs of knots in jets are 3C 277.3 (knots K_1 and K_2; van Breugel *et al.* 1985*a*) and M87 (the brightest knots A and B; Owen, Hardee, and Bignell 1980). In all these objects the knots closest to the nuclei are the most compact, appear edge brightened on the upstream sides, and are elongated perpendicular to the jet directions, while the secondary knots are more diffuse and elongated along the jet. This suggests that after a first strong shock, which heats and expands the jet fluid, a secondary, weaker shock may occur, and that this might be a general feature of jets. We also note that the hotspots in many powerful sources exhibit double knots (Dreher 1981; Laing 1984).

Several possible causes for shocks in jets can be envisaged. They may be due to (*a*) effects internal to the jet and surrounding cocoon, as shown in the model simulations by Norman *et al.* (1982); (*b*) the collision of the jet with external material such as clouds in the ambient interstellar medium, as originally proposed for the jet in M87 by Blandford and Königl (1979); or (*c*) reconfinement of a jet as it responds to a changing external pressure, as perhaps is the case in NGC 315 (Sanders 1983) and M87 (Falle and Wilson 1985). Since the models by Norman *et al.* (1982) are calculated under the assumption of a constant background medium, whereas the radio and optical morphologies of the southern jet and northern lobe suggest substantial interaction with ambient gas (see below), processes (*b*) and (*c*) may be more important than (*a*).

iii) *Deflection of the Northern Jet*

Collisions between a jet and clouds of gas are strongly suggested in the northern lobe of 4C 29.30, as in the southern jet of 3C 277.3, by the bright emission-line regions adjacent to the knots, and by the bent radio appearance downstream from them. The shocks may heat the jet fluid so that the jet expands, slows down, and deflects farther downstream. Unlike 3C 277.3, where the jet shows up as an upolarized feature against the background of its polarized lobe, there is no such clear evidence for entrainment of gas in the northern lobe of 4C 29.30.

We can perform a calculation similar to the one used for the jet in 3C 277.3 to show that the emission-line region is indeed sufficiently massive to deflect the jet. The cloud mass required to deflect the jet may roughly be estimated from the jet thrust, $\dot{M}_j v_j$, which accelerates the cloud (with mass M_c and velocity v_c) in a time t_c: $M_c = \dot{M}_j v_j t_c / v_c$. Since the jet thrust per unit area must be larger than the pressure (P_k) in the radio knot D1, one has $\dot{M}_j v_j > P_k A_k$ (where A_k is the cross sectional area of the knot), so that $M_c > P_k A_k t_c / v_c$. Using the physical parameters for D1 listed in Table 4, and taking $v_c = 200$ km s^{-1} (Fig. 9*a*), we find $M_c > 3.5 \times 10^6 [t_c/(3 \times 10^6)]\ M_\odot$. Here we have normalized t_c with respect to the synchrotron lifetime (at $\lambda = 6$ cm) of the northern lobe D. The "observed" value for M_c is $\sim 3 \times 10^6/(n_e/100)\ M_\odot$ (Table 5), in the form of optically emitting (ionized) gas alone. While the above arguments are rather simple, and the value for t_c is uncertain, the data are at least consistent with the jet being deflected by a massive ambient cloud or complex of clouds.

A more sophisticated analysis of bent jets involves theories of oblique internal shocks (Christiansen, Burns, and Stocke 1984; Henriksen 1984). A model for a jet-cloud "ricochet" interaction, incorporating some of the results from the hydrodynamic simulations by Norman *et al.* (1982), was proposed by Henriksen (1984). In this model a strong shock (Mach disk) with adjacent oblique shocks develops at the cloud collision site. Shocked jet material at the side of the cloud may heat and accelerate the cloud, while on the other side it may escape at a certain angle (θ) relative to the incident jet. For a single oblique shock, $\theta_{\max} = 40°$.

In the northern lobe of 4C 29.30, one might identify D1 with the Mach disk in the jet, and D3 with the part of the jet which is farthest from the cloud NL1 and escaped relatively unharmed until it encountered the next obstacle, NL2. Knot D2 could be a secondary shock at the interface of the part of the jet interacting with the cloud, and the location where the cloud material (NL1) is heated and accelerated. This would be consistent with our observation of line emission extending to the north (Fig. 7*a*) and its large velocity shift there ($\sim +200$ km s^{-1}; Fig. 9*a*).

The projected angle (θ_p) between the brightest radio emission in D3 and the normal to the supposed Mach disk (at D1, P.A. = 133°) is $\sim 14°$. Thus, a single oblique shock would be sufficient to deflect this part of the jet. If the angle between the oblique shock and the jet, as well as all projection angles, were known, one could in principle derive the Mach number of the jet and shock (see Henriksen 1984).

Whatever the details of the jet/cloud interaction, it is clear from the radio observations that the jet is effectively stopped near the bright emission-line regions NL1 and NL2, and that the kinetic energy of the jet is almost entirely dissipated into heating the gas (see § IV*c*).

iv) *Reconfinement Shocks in the Southern Jet?*

The string of knots in the rather straight southern jet of 4C 29.30 might best be explained by shocks that occur within the jet when it readjusts to the varying external pressure while moving outward through the galaxy. Such a model of a reconfining jet in a galactic atmosphere was successfully used by Sanders (1983) to explain the "reconfinement shoulder" in the jet of NGC 315 (Willis *et al.* 1981). It also elegantly predicts the observed location of the brightest knot in the M87 jet (Falle and Wilson 1985). Support for such a model for the southern jet of 4C 29.30 may be that the brightest knot (A2) occurs approximately where the jet exits the main body of the galaxy (Fig. 4) and enters a region of much lower density and pressure.

Beyond this knot the jet decollimates rapidly and merges with a diffuse tail (T) to the SW.

A reconfinement model for a jet can yield useful constraints on its Mach number and mass supply rate. However, this requires knowledge of its ambient pressure, and estimates of certain parameters at the base of the jet (Mach number, pressure, and distance from the nucleus where the jet breaks free). It is not clear what would be reasonable assumptions in this regard for 4C 29.30. Estimates of the jet velocity and internal gas density may also be obtained in several other model-dependent ways; see Perley, Bridle, and Willis (1984) for a summary of the various methods and assumptions involved. One typically finds velocities of several thousand km s^{-1} or more.

Our optical data on the southern emission-line filament in 4C 29.30 give us at least one firm lower limit to the jet velocity: $v_j > 730$ km s^{-1}. This is a lower limit because of projection effects; also, it is unlikely that the velocity of the jet is smaller inside than at its periphery. Models of the transverse velocity profiles of jets, such as those by Henriksen (1986), and De Young (1986), may be used to extrapolate these measurements to an internal jet velocity. Assuming a jet with turbulent boundary layers and an associated entrainment flow, Henriksen (1986) finds a typical internal jet velocity of order 10^4 km s^{-1}, if the velocity at the edges is $\sim 10^3$ km s^{-1}. With such a velocity, the jet would have sufficient kinetic energy to power the radio lobes and emission-line gas.

v) *Polarization*

Near locations with emission-line gas, the percentage polarization (P) of the radio continuum is relatively low (Table 4). Since the gas appears to be located predominantly near the edges of the source, the radio emission is probably being depolarized by an inhomogeneous Faraday screen, as in 4C 26.42, 3C 277.3, and many other objects. If this is true, P should be a strong function of wavelength: $P \propto \exp(-A\lambda^4)$, where A is a parameter that depends on the distribution of Faraday depths in the boundary layer (Burn 1966). It is then somewhat surprising that near component D, P is similar (but low) at both 6 cm and 21 cm [$(DP)_6^{21} = 1.0 \pm 0.1$; Table 4].

A possible explanation is that the radio component may be only partially covered by a screen, and that this partial screen is "Faraday opaque" at 6 cm (and thus also at 21 cm). One might expect that these parts of the screen might become transparent to polarized emission at shorter wavelengths. Unfortunately, our observations at 2 cm have insufficient sensitivity to check this. If we assume that the intrinsic polarization (at $\lambda = 0$) in D is similar to that of component A2, where there is no optical line emission and P is the same ($\sim 35\%$) at all three wavelengths, then the observed value of $\sim 9\%$ at 6 cm in D suggests that the covering factor of cells with significant Faraday rotation is large ($\sim 75\%$).

Regardless of the details of the models, considerable Faraday rotation in a radio-emitting plasma with much ionized (thermal) gas requires that the Faraday depth ($\lambda^2\Phi$ rad) is appreciable, typically $\lambda^2\Phi \gtrsim \pi$ rad (Burn 1966). Here, we have $\lambda^2\Phi = 0.16\lambda^2 B_{\|} n_e f_m l$ rad, where n_e is the thermal electron density (cm^{-3}), $B_{\|}$ is the magnetic field strength (μG) along the line of sight l (kpc) through the radio-emitting region, f_m is the filling factor for the magnetoionic medium, and λ is the radio wavelength (cm).

Two extreme cases can be considered: the Faraday screen consists predominantly of the optical emission-line gas itself, or of irregularities in the intercloud medium. With a rather large number of assumptions, it is possible to evaluate which of these two explanations is the most plausible. Taking component D with its associated optical emission-line region NL1 as an example, and assuming $B_{\|} \approx 100$ μG (Table 4B) and $l \approx 1$ kpc in both cases, we can write the Faraday depth at $\lambda = 6$ cm as $\lambda^2\Phi \approx 600 n_e f_m$ rad.

If the Faraday screen is caused purely by the emission-line gas, and if $f_m \approx f_f \approx 0.4 \times 10^{-6}$ and $n_e \approx 240$ cm^{-3} (Table 7B), then $n_e f_m \approx 1 \times 10^{-4}$ and $\lambda^2\Phi \approx 0.06$ rad. Within the framework of our assumptions, this appears insufficient to produce considerable Faraday depolarization. On the other hand, if the screen is caused by irregularities in the intercloud medium, then $f_m \approx 1$, and the requirement $\lambda^2\Phi \approx 600 n_e f_m \gtrsim \pi$ translates into $n_e \gtrsim 0.005$ cm^{-3}. This is a reasonable lower limit to a "typical" intercloud medium such as that in our own Galaxy.

Although many assumptions were made in these simple calculations, it appears that the bulk of the depolarization in the Faraday screen might be caused by irregularities in the intercloud medium, rather than by the optical emission-line gas itself. A plausible origin for these irregularities would be turbulence associated with the entrainment of ambient gas by the radio source.

The constancy of the Faraday rotation across the source ($\sim +60°$ between 6 cm and 21 cm, subject to ambiguities of 180°) suggests that it is caused by a large-scale, homogeneous foreground screen, most likely associated with our own Galaxy. A rotation of $+60°$, the minimum value, corresponds to a Galactic rotation measure of $+27$ rad m^{-2}, consistent with values found by Simard-Normandin and Kronberg (1979) for this part of the Galaxy. This also means that the thermal gas densities within 4C 29.30 are probably low; in a simple slab model (Burn 1966), the absence of intrinsic Faraday rotation in A2, for example, would imply that $n_e \ll 0.01$ cm^{-3}. The very small amount of ionized gas within radio galaxies may be a rather general phenomenon (Spangler and Sakurai 1985).

We note that in 4C 29.30 the small, relatively bright radio components with low polarization (D1, D2) are apparently embedded in larger, more diffuse, and more highly polarized regions. As we suggested for the similar case of 3C 171, this geometry might naturally arise as a result of the interaction of a jet with a cloudy medium. The collision creates shocks which appear as radio knots within the jet, and which are depolarized by the clumpy ionized gas entrained in the boundary layers. It also causes the jet to deflect and decollimate (due, for instance, to the internal heating by the shocks), so that diffuse radio-emitting plasma may be sprayed out and seen in projection against the unpolarized knots. Alternatively, the unpolarized knots may be seen in projection against the diffuse lobes, as seems to be the case in 3C 277.3.

V. CONCLUSIONS

The radio and optical properties of 4C 29.30 resemble those in other well-documented cases of morphological associations between radio jets, lobes, and spatially extended regions of optical emission-line gas. 4C 29.30, however, is particularly instructive in a number of ways.

One example is that the origin of the emission-line gas seems clear in 4C 29.30: evidence that the parent galaxy has captured a gas-rich disk galaxy, perhaps very recently, is strong. The faint optical shells, the secondary blue nucleus, the circumnuclear dust band, and the blue component of the stellar population all support this idea. Such a galaxy merger would have

supplied the parent galaxy of 4C 29.30, which was possibly a normal elliptical prior to the merger, with an interstellar medium full of relatively dense, cool clouds. We propose that the clouds were then excited by the radio jets as they traveled out through this debris. Indeed, the identification of peculiar, merging galaxies with radio sources, several of which are associated with optical emission-line regions, seems to be a much more common phenomenon than is often assumed (Heckman *et al.* 1985). We believe that these data strongly support the hypothesis that the emission-line gas associated with radio jets is ambient material, not ejecta from the nucleus. Other, more general, reasons for believing this are discussed by van Breugel *et al.* (1985*a*).

The data confirm our earlier conclusion that Faraday depolarization of radio continuum emission may be produced by "Faraday screens" consisting of lumpy gas embedded in, and entrained by, the boundary layers of radio sources. This gas need not always be visible as optical line emission: simple calculations suggest that most of the depolarization may actually be caused by a turbulent intercloud medium, rather than by the emission-line gas itself.

Our radio and optical data on 4C 29.30 thus provide clear evidence that the ambient medium can be very important in determining the properties of a radio source. Of special interest is the apparent jet/cloud collision occurring in the northern radio lobe. The close association of the bright radio knots with the optically emitting clouds supports models in which radio emission may be produced through shocks located at the collision sites. The subsequent bending and decollimation of the jet, which apparently occurs downstream, implies that such collisions may also be responsible for many of the observed distortions in other radio sources.

The knotty structure in the rather straight southern jet of 4C 29.30 seems to suggest a different explanation. In this part of the source, the jet may not have encountered very dense clouds directly along its path, and we may be witnessing the effects of shocks responding to pressure changes within the jet as it adjusts to a rapidly diminishing external pressure in the galaxy.

The large misalignment between the southern jet and the optical filament is puzzling, but the dramatic increase in velocity near the southern hotspot implies that the jet and gas are interacting. In fact, the projected velocity at the end of this feature is so large (~ 730 km s^{-1}) that gas is likely to be leaving its parent galaxy, since the escape velocity is a few hundred km s^{-1}. Although entrainment of galactic gas by a radio jet is an unexpected way to enrich the intergalactic medium, this appears to be occurring in 4C 29.30! In addition, the absence of bright radio emission between the jet and filament suggests that there may be more to radio jets than meets the (radio) eye. It could be that the radio jet is only the high-energy part of a much larger outflow which surrounds the jet, perhaps analogous to stellar jets and their associated bipolar outflows.

4C 29.30 also illustrates how the ambient medium may be affected by a radio source. The peculiar kinematics of the gas (e.g., the large velocity discontinuities and broad lines near the edges of bright radio components) clearly suggest the interaction of the jets and lobes with the surrounding gas. The velocities are almost certainly not representative of material within the jets themselves, but they do provide information about entrainment of ambient gas in their boundary layers. The large velocity gradient along the filament in the vicinity of the southern hotspot shows that a jet may disrupt and accelerate surrounding gas even at a considerable distance ($\sim 8''$, or ~ 9 kpc) from its center.

The inadequacy of the continuum from the nucleus to photoionize the emission-line gas in the northern radio lobe, together with the clear morphological relation between the radio-emitting plasma and the gas, implies that the jets which power the radio emission must also heat and ionize the emission-line gas. While the mechanism by which this occurs is not clear, the fact that the total emission-line luminosity is at least a factor of ~ 10 higher than the radio luminosity of the lobe implies that the jet dissipates only a very small fraction ($\lesssim 10\%$) of its energy in the form of radio synchrotron emission. This result is not unexpected on theoretical grounds. The observational input provided by 4C 29.30, and by other objects in which most of the jet's energy is dumped into a dense interstellar medium and processed into optical emission-line photons, may be of use to general questions concerning the energetics of radio sources.

Finally, radio and optical observations such as those presented here reveal that the interaction of radio galaxies with ambient dense gas may be quite complex. The relationship between the emission-line gas and the radio source is indirect, and gives information only on the boundaries (cocoons, lobes) of the jets. To fully take advantage of the wealth of optical information, and to relate these measurements to the internal properties (velocity, density) of the jet, further theoretical work on the entrainment of ambient gas by jets is necessary.

We wish to thank the staffs of the VLA, Kitt Peak National Observatory, Steward Observatory, and Lick Observatory for their assistance in obtaining and reducing the data. We are particularly grateful for the absentee observing and calibration service provided by the VLA staff. Useful discussions with Drs. A. H. Bridle, C. A. Norman, R. E. Pudritz, and A. S. Wilson are acknowledged.

The research of W. J. M. v. B. is supported by National Science Foundation (NSF) grant AST 84-16177. T. M. H. thanks the Alfred P. Sloan Foundation and the NSF, the latter for support under grant AST 82-16553. G. K. M. acknowledges partial travel support from NATO grant 1828, and A. V. F. is grateful to the Miller Institute for Basic Research in Science (U. C. Berkeley) for a postdoctoral fellowship.

The VLA is a facility of the National Radio Astronomy Observatory, which is operated by the Associated Universities, Inc., under contract with the NSF. Kitt Peak National Observatory is a facility of the National Optical Astronomy Observatories, operated by the Association of Universities for Research in Astronomy under contract with the NSF.

REFERENCES

Allen, D. A. 1979, *M.N.R.A.S.*, **186**, 1P.
Baldwin, J. A., Phillips, M. M., and Terlevich, R. 1981, *Pub. A.S.P.*, **93**, 5.
Begelman, M. C., Blandford, R. D., and Rees, M. J. 1984, *Rev. Mod. Phys.*, **56**, 255.
Biretta, J. A., Owen, F. N., and Hardee, P. E. 1983, *Ap. J. (Letters)*, **274**, L27.
Blandford, R. D., and Königl, A. 1979, *Ap. Letters*, **20**, 15.
Blandford, R. D., and Payne, D. G. 1982, *M.N.R.A.S.*, **199**, 883.
Burn, B. J. 1966, *M.N.R.A.S.*, **133**, 67.
Burns, J. O., Owen, F. N., and Rudnick, L. 1979, *A.J.*, **84**, 1983.
Burstein, D., and Heiles, C. 1982, *A.J.*, **87**, 1165.
Cantó, J., Elliott, K. H., Meaburn, J., and Theokas, A. C. 1980, *M.N.R.A.S.*, **193**, 911.

Christiansen, W. A., Burns, J. O., and Stocke, J. T. 1984, in *Proc. Green Bank Workshop on Jets*, ed. A. H. Bridle and J. Eilek (Charlottesville: NRAO), p. 83.
Cohen, R. D., and Osterbrock, D. E. 1981, *Ap. J.*, **243**, 81.
Colla, G., Fanti, C., Fanti, R., Lari, C., Lequeux, J., Lucas, R., and Ulrich, M.-H. 1975, *Astr. Ap. Suppl.*, **20**, 1.
De Veny, J. B. 1983, *An Observer's Manual for the Cryogenic Camera* (Tucson: Kitt Peak National Observatory).
De Young, D. S., 1986, *Ap. J.*, **307**, 62.
Dreher, J. W. 1981, *A.J.*, **86**, 833.
Dreher, J. W., and Feigelson, E. D. 1984, *Nature*, **308**, 43.
Duric, N., Seaquist, E. R., Crane, P. C., Bignell, R. C., and Davis, L. E. 1983, *Ap. J. (Letters)*, **273**, L11.
Falle, S. A. E. G., and Wilson, M. J. 1985, *M.N.R.A.S.*, **216**, 79.
Fanti, C., Fanti, R., Gioia, I. M., Lari, C., Parma, P., and Ulrich, M.-H. 1977, *Astr. Ap. Suppl.*, **29**, 279.
Ferland, G. J., and Mushotzky, R. F. 1984, *Ap. J.*, **286**, 42.
Ferland, G. J., and Netzer, H. 1983, *Ap. J.*, **264**, 105.
Filippenko, A. V. 1985, *Ap. J.*, **289**, 475.
Filippenko, A. V., and Halpern, J. P. 1984, *Ap. J.*, **285**, 458.
Filippenko, A. V., and Sargent, W. L. W. 1985, *Ap. J. Suppl.*, **57**, 503.
———. 1986, in *Structure and Evolution of Active Galactic Nuclei*, ed. G. Giuricin *et al.* (Dordrecht: Reidel), p. 21.
Ford, W. K., Jr. 1979, *Ann. Rev. Astr. Ap.*, **17**, 189.
Graham, J. A., and Price, R. M. 1981, *Ap. J.*, **247**, 813.
Halpern, J. P., and Filippenko, A. V. 1984, *Ap. J.*, **285**, 475.
Halpern, J. P., and Steiner, J. E. 1983, *Ap. J. (Letters)*, **269**, L37.
Heckman, T. M. 1980*a*, *Astr. Ap.*, **87**, 142.
———. 1980*b*, *Astr. Ap.*, **87**, 152.
———. 1981, *Ap. J. (Letters)*, **250**, L59.
Heckman, T. M., Miley, G. K., Balick, B., van Breugel, W. J. M., and Butcher, H. R. 1982, *Ap. J.*, **262**, 529.
Heckman, T. M., Miley, G. K., van Breugel, W. J. M., and Butcher, H. R. 1981, *Ap. J.*, **247**, 403.
Heckman, T. M., Smith, E. P., Baum, S. A., van Breugel, W. J. M., and Balick, B., 1986, preprint.
Heckman, T. M., van Breugel, W. J. M., and Miley, G. K. 1984, *Ap. J.*, **286**, 509.
Henriksen, R. N. 1984, in *Proc. Green Bank Workshop on Jets*, ed. A. H. Bridle and J. Eilek (Charlottesville: NRAO), p. 122.
———. 1986, preprint.
Hernquist, L., and Quinn, P. J. 1986*a*, *Ap. J.*, in press.
———. 1986*b*, *Ap. J.*, in press.
Killeen, N. E. B., Bicknell, G. V., and Ekers, R. D. 1986, preprint.
Koski, A. T. 1978, *Ap. J.*, **223**, 56.
Kotanyi, C. G., and Ekers, R. D. 1979, *Astr. Ap.*, **73**, L1.
Laing, R. A. 1984, in *Proc. Green Bank Workshop on Jets*, ed. A. H. Bridle and J. Eilek (Charlottesville: NRAO), p. 128.
Lonsdale, G. J., Helou, G., Good, J. C., and Rice, W. 1985, *Catalogued Galaxies and Quasars Observed in the IRAS Survey*, Jet Propulsion Laboratory publication.
Malin, D. F., and Carter, D. 1983, *Ap. J.*, **274**, 534.
Malkan, M. A., and Filippenko, A. V. 1983, *Ap. J.*, **275**, 477.
Malkan, M. A., and Sargent, W. L. W. 1982, *Ap. J.*, **254**, 22.
Marcus, S. L., Nelson, R. E., and Lynds, C. R. in *Instrumentation in Astronomy III*, (*Proc. S.P.I.E.*, Vol. **172**), p. 207.
McCray, R., and Snow, T. P., Jr. 1979, *Ann. Rev. Astr. Ap.*, **17**, 213.
McKee, C. F., and Hollenbach, D. J. 1980, *Ann. Rev. Astr. Ap.*, **18**, 219.
Merritt, D., and de Zeeuw, T. 1983, *Ap. J. (Letters)*, **267**, L19.
Miley, G. K. 1983, in *Astrophysical Jets*, ed. A. Ferrari and A. G. Pacholczyk (Dordrecht: Reidel), p. 99.
Miley, G. K., Heckman, T. M., Butcher, H. R., and van Breugel, W. J. M. 1981, *Ap. J. (Letters)*, **247**, L5.
Miller, J. S. 1983, *The Lick 3 m Cassegrain CCD Spectrograph* (Santa Cruz: Lick Observatory).
Miller, J. S., Robinson, L. B., and Wampler, E. J. 1976, *Adv. Electronics Electron Phys.*, **40B**, 693.
Norman, M. L., Smarr, L., Winkler, K.-H., and Smith, M. D. 1982, *Astr. Ap.*, **113**, 285.
O'Dea, C. P. 1985, *Ap. J.*, **295**, 80.
Owen, F. N., Hardee, P. E., Bignell, R. C. 1980, *Ap. J. (Letters)*, **239**, L11.
Owen, F. N., Rudnick, L., and Peterson, B. M. 1977, *A.J.*, **82**, 677.
Perley, R. A., Bridle, A. H., and Willis, A. G. 1984, *Ap. J. Suppl.*, **54**, 291.
Pudritz, R. E., and Norman, C. A. 1986, in *Proc. Toronto Conference on Jets from Stars and Galaxies*, ed. R. N. Henriksen, and T. W. Jones (*Canadian Journal of Physics*, **64**), p. 501.
Quinn, P. J. 1984, *Ap. J.*, **279**, 596.
Robinson, W., Ball, W., Vokac, P., Piegorsch, W., and Reed, R. 1979, *Instrumentation in Astronomy III* (*Proc. S.P.I.E.*, Vol. **172**), p. 98.
Sanders, R. H. 1983, *Ap. J.*, **266**, 73.
Shectman, S. A. 1981, in *Ann. Rept. Dir. Mt. Wilson and Las Campanas Observatories* (Washington: Carnegie Institution of Washington), p. 586.
Shull, J. M., and McKee, C. F. 1979, *Ap. J.*, **227**, 131.
Simard-Normandin, M., and Kronberg, P. P. 1979, *Nature*, **279**, 115.
Simkin, S. M., Bicknell, G. V., and Bosma, A. 1984, *Ap. J.*, **277**, 513.
Smarr, L. L., Norman, M. L., and Winkler, K.-H. 1984, in *Physica*, **5**, 83.
Spangler, S. R., and Sakurai, T. 1985, *Ap. J.*, **297**, 84.
Thompson, A. R., Clark, B. G., Wade, C. M., and Napier, P. J. 1980, *Ap. J. Suppl.*, **44**, 151.
Toomre, A., and Toomre, J. 1972, *Ap. J.*, **178**, 623.
Uchida, Y., Kaifu, N., Shibata, K., Hayashi, S. S., and Hasegawa, T. 1986, in *IAU Symp. 115, Star-Forming Regions*, in press.
van Breugel, W. J. M. 1986, in *Proc. Toronto Conference on Jets from Stars and Galaxies*, ed. R. N. Henriksen and T. W. Jones (*Canadian Journal of Physics*, **64**), p. 392.
van Breugel, W. J. M., Filippenko, A. V., Heckman, T. M., and Miley, G. K. 1985*b*, *Ap. J.*, **293**, 83.
van Breugel, W. J. M., and Fomalont, E. B. 1984, *Ap. J. (Letters)*, **282**, L55.
van Breugel, W. J. M., and Heckman, T. M. 1982, in *IAU Symposium 97, Extragalactic Radio Sources*, ed. D. S. Heeschen and C. M. Wade (Dordrecht: Reidel), p. 61.
van Breugel, W. J. M., Heckman, T. M., and Miley, G. K. 1984, *Ap. J.*, **276**, 79.
van Breugel, W. J. M., Miley, G. K., and Heckman, T. M. 1984, *A.J.*, **89**, 5.
van Breugel, W. J. M., Miley, G. K., Heckman, T. M., Butcher, H. R., and Bridle, A. H. 1985*a*, *Ap. J.*, **290**, 496.
Williams, R. E., and Christiansen, W. A. 1985, *Ap. J.*, **291**, 80.
Willis, A. G., Strom, R. G., Bridle, A. H., and Fomalont, E. B. 1981, *Astr. Ap.*, **95**, 250.
Yee, H. K. C., and Oke, J. B. 1978, *Ap. J.*, **226**, 753.

ALEXEI V. FILIPPENKO: Department of Astronomy, University of California, Berkeley, CA 94720

TIMOTHY M. HECKMAN: Astronomy Program, University of Maryland, Space Science Building, College Park, MD 20742

GEORGE K. MILEY: Space Telescope Science Institute, Homewood Campus, Baltimore, MD 21218

WIL J. M. VAN BREUGEL: University of California, Radio Astronomy Laboratory, 601 Campbell Hall, Berkeley, CA 94720